Demagnetization of terrestrial and extraterrestrial rocks under hydrostatic pressure up to 1.2GPa

Natalia S. Bezaeva, Jérôme Gattacceca, Pierre Rochette, Ravil A. Sadykov, Vladimir I. Trukhin

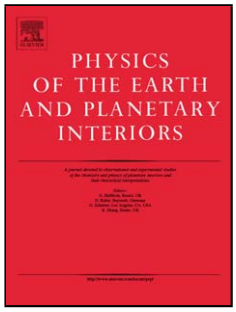

Title: Demagnetization of terrestrial and extraterrestrial rocks under hydrostatic pressure up to 1.2 GPa

Authors: Natalia S. Bezaeva, Jérôme Gattacceca, Pierre Rochette, Ravil A. Sadykov, Vladimir I. Trukhin

PII: S0031-9201(10)00007-5
DOI: doi:10.1016/j.pepi.2010.01.004
Reference: PEPI 5238

To appear in: *Physics of the Earth and Planetary Interiors*

Received date: 14-5-2009
Revised date: 9-12-2009
Accepted date: 8-1-2010

Please cite this article as: Bezaeva, N.S., Gattacceca, J., Rochette, P., Sadykov, R.A., Trukhin, V.I., Demagnetization of terrestrial and extraterrestrial rocks under hydrostatic pressure up to 1.2 GPa, *Physics of the Earth and Planetary Interiors* (2008), doi:10.1016/j.pepi.2010.01.004

Demagnetization of terrestrial and extraterrestrial rocks under hydrostatic pressure up to 1.2 GPa

Natalia S. Bezaeva [a,b*], Jérôme Gattacceca [a], Pierre Rochette [a], Ravil A. Sadykov [c,d] and Vladimir I. Trukhin [b]

[a] CEREGE, CNRS/Aix-Marseille Université, BP 80, 13545, Aix en Provence, Cedex 4, France

[b] Faculty of Physics, M.V. Lomonosov Moscow State University, Leninskie gory, 119991, Moscow, Russia

[c] Institute for Nuclear Research, Russian Academy of Sciences, 60-let Oktyabrya pr. 7a, 117312, Moscow, Russia.

[d] Institute for High Pressure Physics, Russian Academy of Sciences, Kaluzhskoye sh. 14, 142190, Troitsk, Russia

Abstract

We carried out hydrostatic pressure demagnetization experiments up to 1.24 GPa on samples of terrestrial and extraterrestrial rocks and minerals of different lithologies as well as on synthetic samples. The magnetic remanence of samples was measured directly under pressure using a non-magnetic high pressure cell of piston-cylinder type that was inserted into a high sensitivity SQUID magnetometer. In order to bring light on the pressure demagnetization effect, we investigated 50 samples with different magnetic mineralogies, remanent coercivities (B_{cr}) and hysteresis parameters. The samples consisted of pyrrhotite-, magnetite- and titanomagnetite-bearing Martian meteorites, taenite-, tetrataenite and kamacite-bearing ordinary chondrites and pyrrhotite-bearing Rumuruti chondrite; magnetite- and titanomagnetite-bearing basalts, andesites, ignimbrites, obsidians and granites; a variety of pyrrhotite- and hematite-bearing rocks and minerals (jasper, schist, rhyolite, radiolarite); samples of goethite and greigite as well as synthetic samples of dispersed powders of magnetite, hematite, pyrrhotite and native iron set into epoxy resin. Under hydrostatic pressure of 1.24 GPa, applied in a low magnetic field (<5μT), the samples lost up to 84% of their initial saturation isothermal remanent magnetization (SIRM) without any changes in their intrinsic magnetic properties. We found that the efficiency of the pressure demagnetization is not exclusively controlled by the magnetic hardness of the samples (B_{cr}), but that it is strongly dependent on their magnetic mineralogy. For a given magnetic mineralogy the resistance to hydrostatic pressure is roughly proportional to ln(B_{cr}). It was shown that there is no simple equivalence between pressure demagnetization and alternating field demagnetization effects. The

* Corresponding author. Tel.: +7-4959393848; fax: +7-4959394881. *E-mail addresses:* bezaeva@physics.msu.ru (N.S. Bezaeva), gattacceca@cerege.fr (J. Gattacceca), rochette@cerege.fr (P. Rochette), rsadykov@inr.ru (R.A. Sadykov), trukhin@phys.msu.ru (V.I. Trukhin).

pressure demagnetization was shown to be time-independent but repeated application of the same pressure level resulted in further demagnetization.

Keywords: Pressure demagnetization; Hydrostatic pressure; Remanent magnetization; Rock magnetism

1. Introduction

Hypervelocity impacts are a major mechanism for the evolution of the solid matter in our solar system. Shock waves generated during impacts can modify both intrinsic magnetic properties (Gattacceca et al., 2007a; Louzada et al., 2007; Nishioka et al., 2007; Gilder et al., 2008) and remanent magnetization (Pohl, 1975; Kletetschka et al., 2004; Gattacceca et al., 2006, 2008; Louzada et al., 2007) of rocks. Consequently, the magnetic record of solid bodies in the solar system, affected by impacts to different degrees, could have been erased or overprinted by shock events. Understanding the process and the physical mechanism of the impact remagnetization is therefore a key issue to the interpretation of the crustal magnetization of Mars (Hood et al., 2003, 2009), the Moon (Cisowski et al., 1976; Halekas et al., 2002, 2003), small solid solar system bodies such as asteroids (Chen et al., 1995) as well as paleomagnetic records of meteorites and extraterrestrial materials available from sample return. Concerning the Earth, shock-induced changes in rock magnetic properties and magnetic remanence should be taken into consideration while studying the remanent magnetism of terrestrial impacts (Halls, 1979; Pesonen et al., 1992; Pilkington and Grieve, 1992; Louzada et al., 2008).

Different authors have carried out experimental investigations of shock demagnetization (remagnetization) of rocks and pure minerals in the 1-30 GPa peak pressure range. Different techniques have been used for shock waves generation: air or gas gun accelerating aluminium or copper projectiles (Hornemann et al., 1975; Pohl et al., 1975; Martelli and Newton, 1977; Cisowski and Fuller, 1978; Srnka et al., 1979; Dickinson and Wasilewski, 2000; Louzada et al., 2007); high explosive and nuclear charges (Hargraves and Perkins, 1969; Pesonen et al., 1997;

Gattacceca et al., 2007a); free falling mass (Kletetschka et al., 2004) and pulsed laser (Gattacceca et al., 2006, 2008). The main caveats of such experiments are the complexity of dynamic pressure calibration, the possible mechanical damages of investigated samples, and deciphering of the effect of deviatoric versus hydrostatic stresses. Indeed, it is known that remanent magnetization is more sensitive to non-hydrostatic (deviatoric) than hydrostatic stresses (Nagata, 1966; Martin and Noel, 1988). Moreover, shock may permanently modify the intrinsic magnetic properties (e.g., coercivity, see Gattacceca et al., 2007a) thus complicating the interpretation.

As for meteorites, considering the relative rarity of extraterrestrial material on the Earth, it is excluded for most of them to perform shock experiments that are not only destructive but also require rather large sample volume. Numerous parameters must be considered when studying the effect of shock on the magnetic remanence: shock intensity and duration, background magnetic field during the shock event, magnetic mineralogy, pre-shock magnetization and temperature. This large number of parameters, that are sometimes difficult to control, complicates the comprehension of shock effect on rock magnetic remanence.

Static pressure experiments are well suited to tackle these problems. They allow better pressure calibration and can be non-destructive for samples. However, they were until recently limited to the low pressure range for under pressure measurements (<0.1 GPa, e.g., Pozzi, 1973). Experiments were also carried out by pressurizing the sample up to 2 GPa, and remeasuring the remanence outside the pressurizing device (Pearce and Karson, 1988). More recently Rochette et al. (2003) compressed a pyrrhotite sample up to 3 GPa in a piston-cylinder press and remeasured isothermal remanent magnetization (IRM) after pressure release. It was found that pyrrhotite undergoes a high pressure magnetic transition under a pressure of 2.8 GPa, which results in a complete loss of its magnetic remanence. This experimental scheme has the disadvantage of needing a new sample and few days of experiments per each pressure value. Moreover, these experiments, by using a solid confining media, generate some deviatoric stress on the sample.

Gilder et al. (2006) performed IRM measurements of pure single domain (SD) and multidomain (MD) magnetite under quasihydrostatic load up to 4.2 GPa using a diamond anvil non-magnetic cell (in the Earth's magnetic field) and also observed a pressure demagnetization effect. Gilder and Le Goff (2008) carried out pressure experiments up to 6 GPa using a moissanite anvil cell on natural and synthesized MD titanomagnetite with different titanium concentration, but this work was focused upon the influence of stress on the acquisition of IRM. All these experiments are restricted to pure strongly magnetic minerals due to the minute sample size (e.g., for the diamond anvil cell the cylindrical sample chamber was 400 μm in diameter and 100 μm in height) and cannot be realized on bulk rock samples without extracting their magnetic fraction.

Pressure demagnetization experiments on bulk rock samples have significant implications in solid-state physics and geophysics, in particular in paleomagnetism and interpretation of crustal magnetic anomalies of the solid Solar System bodies. As crustal rocks suffer the load created by overlying rocks and/or water column (for instance ~0.06 GPa for 5 km of water and 350 m of sediments), laboratory studies of the effect of pressure on the remanent magnetism of rocks may be helpful for the comprehension and interpretation of the paleomagnetic signal of the deep seated rocks and crustal magnetic anomalies. However, together with pressure, crustal rocks undergo the concomitant influence of high temperatures, making the situation even more complex. At pressures up to 1.5 - 2 GPa, which corresponds to a crustal thickness of 50-70 km, titanomagnetites do not crystallize any more (Valeev, 1984): this is the upper limit of relevant pressures.

Despite previous works, the effect of pressure on the remanent magnetization is still poorly known for natural materials for pressures of the order of 1 GPa. The goal of this work is to present a thorough investigation of the effect of hydrostatic pressure up to 1.24 GPa on the magnetic remanence of rocks within a wide range of magnetic mineralogies. We investigated 50 samples of terrestrial and extraterrestrial rocks and minerals as well as synthetic samples with the

following magnetic carriers: magnetite, titanomagnetite, hematite, pyrrhotite, native iron and nickel iron, goethite, greigite. For each magnetic mineralogy we studied different samples spanning a wide range of remanent coercivity (B_{cr}).

2. Samples and Measuring Techniques

2.1. Experimental Setup

In order to isolate the pressure demagnetization effect on rock magnetic remanence from the creation of piezo-remanent magnetization after pressure application (studied in many previous works, e.g., Nagata, 1966; Kinoshita, 1968; Pozzi, 1973) we always applied the pressure in a low magnetic field (<5 μT).

The experimental setup was designed for room temperature measurements of magnetic remanence of relatively large rock samples (up to 5.8 mm in diameter and 15 mm long cylinders) under hydrostatic pressure up to 1.24 GPa. We used a non-magnetic composite high-pressure cell of piston-cylinder type with an inner diameter of 6 mm allowing direct measurement in a SQUID magnetometer (Fig.1). The cell was made of titanium alloy and "Russian alloy" ($Ni_{57}Cr_{40}Al_3$). Samples were placed into a teflon capsule locked with a teflon plug and filled with inert polyethylsiloxane (PES-1) liquid allowing converting the uniaxial pressure on the pistons into a pure hydrostatic pressure (Kirichenko et al. 2005). Pressure inside the cell was calibrated with a manganin pressure sensor. Details of the cell design can be found in Sadykov et al. (2008).

After loading of the cell with a press (Graseby Specac 15011), pressure was locked inside the cell. The press with the cell inside was placed at the center of three pairs of perpendicular Helmholtz coils connected to stabilized DC supplies. Due to the presence of mobile metallic parts in the press, it was not possible to obtain a stable very low ambient field. The magnetic field in the area of the investigated sample was monitored using a 3 axis flux-gate magnetometer and was always below 5 μT. Measurements of the magnetic moment of the sample under

pressure were performed by inserting the pressure cell containing the sample in a 2G Enterprises SQUID magnetometer. This magnetometer allowed measuring the remanent magnetic moment up to 10^{-4} Am^2 with a noise level of 10^{-11} Am^2.

We investigated the intensity and stability of the magnetic remanence of the cell itself without and under pressure. The remanent magnetic moment of the cell remained stable at $3 \cdot 10^{-8}$ Am^2 at zero pressure and up to $5 \cdot 10^{-8} Am^2$ under pressure in the pressure range 0 to 1.24 GPa, after 5-10 min of relaxation in a magnetically shielded room (ambient field ~100 nT). All measurements of magnetic remanence under pressure presented in this work were performed after 5-10 min of cell relaxation inside the SQUID magnetometer (ambient field 1-2 nT).

In this study the remanence of the investigated samples was always at least one order of magnitude above the remanence of the cell. In most cases, the samples were given a saturation isothermal remanent magnetization (SIRM) in a 3 T magnetic field (9 T for goethite, greigite and hematite-bearing samples) by using a pulse magnetizer MMPM9 from Magnetic Measurements Ltd. before pressure application. A few pressure demagnetization experiments were carried out on a laboratory imparted thermoremanent magnetization (TRM) or a natural remanent magnetization (NRM). The pressure was increased stepwise (8 steps up to 1.24 GPa) and the remanence was measured after each step. The pressure was then released down to zero and the remanence measured again. The specimen was then extracted from the pressure cell and its residual remanence (IRM_{PR}) was demagnetized by alternating field (AF) up to 150 mT and measured using the same cryogenic magnetometer. The sample was then saturated again and was demagnetized by AF. All these measurements were carried out at room temperature.

In some cases the maximum pressure (1.24 GPa) was applied and released several times to check for the effect of repeated loading on the magnetic remanence. In most cases in addition to all the above described measurements, AF demagnetization curves of SIRM before compression were also measured. In our experiments pressure application did not produce any mechanical destruction of the investigated samples.

Before and after pressure application the investigated samples were subjected to standard magnetic analyses. Measurements of low field magnetic susceptibility χ_0 and thermomagnetic curves up to 700 °C were performed with KLY2-CS2 and MFK1-CS3 Agico apparatus (we used different subsamples for heating experiments). Hysteresis loops at room temperature and remanence measurements were obtained with a Micromag Vibrating Sample Magnetometer (VSM) with maximum applicable magnetic field 1 T. Curie temperatures (T_C) of the investigated samples were obtained from thermo magnetic curves. For titanomagnetite-bearing samples substitution rate (ulvospinel content *x*) was estimated using the corresponding T_C values according to Hunt et al. (1995).

2.2. Description of Samples

Pressure demagnetization experiments were carried out on samples of meteorites, terrestrial rocks and minerals as well as synthetic samples with the most common magnetic carriers (titanomagnetite $Fe_{3-x}Ti_xO_4$; magnetite Fe_3O_4; hematite Fe_2O_3; pyrrhotite $Fe_{1-x}S$; goethite FeOOH; greigite Fe_3S_4; kamacite ~$Fe_{0.9}Ni_{0.1}$; taenite ~$Fe_{0.7}Ni_{0.3}$; tetrataenite ~$Fe_{0.5}Ni_{0.5}$). The main magnetic properties of the investigated samples are presented in Table 1.

We investigated Martian meteorites - (Bezaeva et al., 2007) NWA 998 nakhlite and Los Angeles and NWA 1068 basaltic shergottites, nickel iron-bearing ordinary chondrites - Bensour, Pultusk and Saratov - and a pyrrhotite-bearing Rumuruti chondrite NWA 753.

Regarding terrestrial rocks we investigated mostly igneous rocks: three types of andesites from Sardinia (Italy), *au1b* from Monte Au, *cug1b* from Monte Cugguruntis and *osb10b* from Monte Osilo, and five types of basalts: Pleistocene sample *ba* from the Bas-Vivarais area (France), Pleistocene alkaline sample *bb* from Chanteuges (Haute-Loire, France), Oligocene sample *be* from Ethiopian traps and two unshocked samples (*pd6-2-1*, *pd6-2-4*) from Lonar impact crater (Maharashtra state, India). We have also investigated a Pleistocene obsidian (*kil-2*)

from the Kilimandjaro volcano (Tanzania) as well as four granites from Corsica (France), five samples of ignimbrites (all from Sardinia, *iro8* from Monte Ironi and *mtd5b* from Monte Torru, *ona12* and *spi3301, spi3903* from San Pietro Island) and a sample of jasper (from San Pietro Island, Sardinia) as well as some samples of radiolarite from the French Alps, rhyolite from Esterel range (France) and Precambrian-Ordovician metamorphic schist from Wilson Terrane (Northern Victoria Land, Antarctica). We have also studied a natural hydrothermal fibrous goethite sample GT from Tarn (France) with only 0.42 wt.% of impurities (including 0.16% H_2O; 0.12% SiO_2 and Ca, K, Ga for the >100 ppm elements, after Rochette et al. 2005b), and two samples of pyrrhotite from the Harvard Mineralogical Museum (Cambridge, USA): monocrystal *127037* from Chihauhau, Mexico and monocrystal *98080* from Sudbury (Canada). Two natural samples of SD greigite have also been investigated under pressure. Sample *greig-tw1* comes from the Plio-Pleistocene marine sediments from the Lower Gutingkeng Formation in southwestern Taiwan and sample *greig-it1* is from the upper Pliocene marine sediments from the Valle Ricca section near Rome, Italy.

Synthetic samples were in form of dispersed powders set into epoxy resin. Synthetic samples of monoclinic pyrrhotite had grain size $x(\mu m) \in [75, 100]$ for sample *a* and $x(\mu m) \in [150, 250]$ for sample *b*. Synthetic samples of dispersed powders of magnetite with $x<25$ μm, iron with $x=10$ μm and MD hematite were prepared using epoxy resin Araldite AY 103 by VANTICO. Different mass concentrations (0.3; 0.5; 0.8; 17%, see Table 1) of magnetite powder were used for the preparation of synthetic samples of magnetite in order to check whether the pressure resistance of magnetite is dependent on the magnetic interaction of grains. Mass concentration of synthetic samples of iron and hematite was of 2.5% and 2.1% respectively. For magnetite and iron we assume that clustering is not a serious issue as the grains are multidomain and stiring the viscous loaded resin should be sufficient to destroy magnetic aggregates. While magnetite and iron powders are commercial synthetic products, the hematite powder comes from a natural ore from Elba Island (Italy); the pyrrhotite samples are described in Dekkers (1988).

The typical mass for the investigated rock samples was in the 0.02 to 0.5 g range (Table 1). As one can see from Table 1, we have investigated under pressure numerous samples with different magnetic mineralogies within a wide range of B_{cr} and grain sizes: from single domain, pseudosingle domain (PSD) to multidomain.

3. Experimental results

3.1. Main characteristics of the pressure demagnetization experiments

The used pressure cell is characterised by a relatively low but nonzero remanent magnetic moment (see above). In order to check the need for correction of the magnetic remanence of investigated samples by the cell magnetic remanence, the sample of rhyolite (*rb7a*) was chosen. This sample is the better suited as it was shown to be the least magnetic (initial SIRM inside pressure cell is $5.48 \cdot 10^{-7} Am^2$). Fig. 2 displays the evolution of the magnetic moment of the cell versus pressure (after 5, 10 and 15 min of the cell relaxation in the magnetically shielded room) as well as an uncorrected and vectorially corrected pressure demagnetization curves for *rb7a* sample. As one can see from Fig. 2, the correction in case of the least magnetic sample *rb7a* appears to be negligible. Therefore, pressure demagnetization curves for all other samples (with much higher magnetic remanence, see Table 2) were not corrected for the remanent magnetic moment of the cell.

The reproducibility of our pressure demagnetization experiments was tested in two different ways. Firstly, using exactly the same experimental protocol, we investigated under pressure the magnetic remanence of two subsamples of radiolarite (*radiol-1* and *radiol-2*) and two subsamples of Bensour meteorite (*Bensour-i* and *Bensour-j*) originated from the same bulk samples. The pressure demagnetization curves for the two radiolarite subsamples are very close (Fig. 3). The same holds for Bensour subsamples. The observed minor differences may come from sample heterogeneity as well as from the uncertainty on the applied pressure value.

Secondly, we used twice the same synthetic sample of dispersed powder of magnetite set into epoxy resin (sample *magn6c*, see Table 1) for two successive pressure demagnetization experiments with an identical experimental protocol. The identical pressure demagnetization curves further demonstrate the reproducibility of our experiments.

As mentioned above (see 2.1), we used the eight-step experimental protocol in the pressure range 0 to 1.24 GPa (see Fig. 4a-f). Several experiments were carried out in order to check the possible influence of the chosen experimental protocol (number of pressure steps up to the maximum pressure) on the final pressure demagnetization effect. Figure 5 displays the one-step pressure demagnetization curves of SIRM of microdiorite up to 0.31, 0.62, 0.93 GPa and the eight-step pressure demagnetization curve up to 1.24 GPa. Each curve corresponds to a different microdiorite subsample. As seen from Fig. 5, the pressure demagnetization degree at a given pressure value p is not sensitive to the number of pressure steps up to p. This points to the additivity of partial pressure demagnetization, consistent with previous work (e.g., Pearce and Karson, 1981).

In order to show that in our experiments the pressure demagnetization effect is not dependent on the duration of pressure application, we carried out the following experiment on a sample of basalt *ba* (see Table 1). The sample was imparted an SIRM and was then put under 0.93 GPa, which led to 48% decrease in its initial magnetic remanence. The sample was then left under pressure during eight days; no further decrease of its magnetic remanence was observed. Thus, we conclude that the efficiency of pressure demagnetization is not time-dependent.

Most pressure demagnetization experiments were carried out on magnetically saturated samples (SIRM). It is known that IRM is not equivalent to NRM or laboratory induced TRM in terms of coercivity spectrum (Dunlop and Özdemir, 1997). Therefore, these different types of remanence may not have the same pressure sensitivity. NRM is expected to be more pressure resistant than IRM and TRM as it is generally already partially demagnetized by viscous decay. We carried out pressure demagnetization experiment on IRM, NRM and laboratory induced

TRM of basalts (*ba* and *bb*). NRM was confirmed to be the most pressure resistant remanence (Fig. 6, sample *bb*). Our results also showed that in some cases IRM was more easily demagnetized by hydrostatic pressure than TRM (Fig. 6, sample *ba*), consistent with Avchyan (1967); but this is not a general result (see Fig. 6, sample *bb* and also Pohl et al., 1975).

Hydrostatic pressure of 1.24 GPa did not produce any changes in SIRM of our samples. For example, both AF demagnetization curves of initial (pre-compressed) SIRM and post-compression SIRM of granite sample *bf9804* are identical (Fig. 7). We do not observe any modification of the intrinsic magnetic properties (hysteresis parameters, low field magnetic susceptibility χ_0, B_{cr}) for the pressure range used in this work, since these modifications occur for pressures above several GPa (Gattacceca et al., 2007a; Louzada et al., 2007; Nishioka et al., 2007). Therefore, the grains are not affected by irreversible changes in the crystalline structure. Thus, pressure demagnetization is more likely due to domain wall displacements (irreversible upon decompression). If so, domain walls are more likely reset by a new saturation, as for all investigated samples SIRM before compression was found to be identical to SIRM imparted after decompression.

3.2. Systematic study of the pressure demagnetization effect

Figure 4a to 4f displays curves of IRM under pressure, normalized to initial SIRM, versus pressure up to 1.24 GPa for all investigated samples. Corresponding AF demagnetization curves of SIRM up to 150 mT (peak alternating field) are presented in Fig. 4g to 4l.

As it was shown in Bezaeva et al. (2007) for the Martian meteorites case, pressure sensitivity of rocks is mainly controlled by their magnetic mineralogy. Therefore, demagnetization curves (Fig.4a-f) were grouped by magnetic mineralogies irrespective of sample type (natural or synthetic, terrestrial or extraterrestrial origin etc.).

The effect of permanent pressure demagnetization (decreasing remanence) was observed on all curves of remanent magnetization under pressure versus pressure except for the goethite sample that retains 100% of its initial SIRM under 1.24 GPa (Fig. 4b), followed by a minor decrease in remanent magnetization (2%) after sample decompression. This is coherent with regard to its very high B_{cr} value (>9 T after Rochette et al., 2005b). On the other hand, the maximum value of pressure demagnetization was obtained for a MD magnetite-bearing microdiorite which lost 84% of its initial SIRM under 1.24 GPa (sample *est* in Table 2 where Δ is the percentage of demagnetization of the initial SIRM under 1.24 GPa).

Among the investigated pyrrhotite-bearing samples (Fig. 4a), PSD sample NWA 753 (Rumuruti chondrite) was found to be the most pressure resistant and synthetic samples of dispersed PSD pyrrhotite powder (*pyr-a* and *pyr-b*) were shown to be the most pressure sensitive. The monocrystal of predominately SD pyrrhotite (sample 98080) has a non-linear behavior resulting in a sharp decrease of IRM above 1.1 GPa. This could be related to a high anisotropy of the sample (Louzada et al., 2009) or/ and the approach to the magnetic phase transition pressure. SD greigite samples lost 10% and 26% of their initial remanent magnetization under pressure, respectively.

In the group of hematite-bearing samples the most pressure sensitive was the synthetic sample of MD hematite that lost Δ=58% of its initial SIRM under pressure, much more than SD hematite sample (Δ=38%), PSD rhyolite (Δ=27%), and radiolarites or jasper ($\Delta \in [30; 35]$%). SD and MD hematite samples have the same provenance (see 2.2): fine grain fraction of SD hematite powder was obtained by crushing the corresponding MD hematite powder (natural ore).

In the group of iron- and nickel iron-bearing samples the synthetic MD iron sample was found to be the most pressure sensitive (Δ=83%) while the tetrataenite-bearing samples (*Saratov* and *Bensour-j* meteorites) are very resistant to pressure (Δ~3%). It is interesting to mention that within the group of $Fe_{1-y}Ni_y$-bearing samples pressure demagnetization degree decreases almost

linearly with increasing Ni-content (y=0% for pure iron, y~10% for kamacite, y~30% for taenite and y~50% for tetrataenite). Additional work is needed to confirm this observation.

In the group of titanomagnetite-bearing samples (Fig. 4d) we investigated samples with different ulvospinel content (x) ranging from x=0.03 (*ona12* and *spi3301*) to x=0.63 (*kil-2*). Pressure sensitivity of titanomagnetites does not seem to be dependent on ulvospinel content alone. For instance, samples *pd6-2-4* and *au1b* have very different x values (x=0.42 and x=0.09, respectively) but have almost the same pressure demagnetization degree under 1.24 GPa.

The group of magnetite-bearing samples shows the most diversified pressure demagnetization behavior and the highest dispersion in Δ under 1.24 GPa with values ranging from 5 to 84%. As seen from Fig.4e-f, some pressure demagnetization curves are almost indistinguishable (e.g., samples *bf8703*, *NWA 998* and *iro8*), in agreement with their similar grain size (PSD, see Table 1) and magnetic hardness ($B_{cr} \in [41, 61]$ mT). Their different geological origin (*bf8703* is a granite and *iro8* is an ignimbrite and *NWA 998* is a mafic cumulate) does not seem to play any significant role with respect to pressure sensitivity.

The values of median destructive field (MDF_i in mT) and median destructive stress (MDS in GPa) of SIRM, needed to remove one half of the initial SIRM by alternating field and by pressure, respectively, are presented in Tables 1-2. Most of MDS values were obtained by linear extrapolation of the linear parts of pressure demagnetization curves. Such values are indicated in italic in Table 2. This computation assumes that pressure demagnetization curves above 1.24 GPa remain linear, and that the samples do not undergo any phase transitions at pressures lower than MDS. It is not the case for pyrrhotite that undergoes a high-pressure magnetic transition and loses 100% of its remanence at about 2.8 GPa (Rochette et al., 2003). On average, hematite-bearing samples have the lowest MDS values situated in 1.1 to 2.3 GPa range (see Table 2).

As it is seen from Fig.4, there is a variety of behaviors with respect to pressure demagnetization. In order to characterize different shapes of pressure demagnetization curves we introduced the following coefficient:

$$\alpha=[(SIRM_0-IRM_{p1})/(SIRM_0-IRM_{p2})]/[p_1/p_2] \quad (1)$$

where $SIRM_0$ is the initial SIRM of the sample in the pressure cell before pressure application, IRM_{p1} is IRM under p_1=0.46 GPa and IRM_{p2} is IRM of the sample under p_2=1.24 GPa. Pressure demagnetization curve has concave shape if α >1, convex shape if α <1 and linear shape if $\alpha\approx1$. As seen from Table 2 and Fig.4, pressure demagnetization curves of magnetite- and titanomagnetite-bearing sample have mostly linear or concave shapes (average α=1.4 for titanomagnetites and 1.5 for magnetites) whereas those of pyrrhotites (except synthetic samples *pyr-a* and *pyr-b*) have slightly convex shape (average α=0.8 without considering synthetic pyrrhotites) due to the existence of a 2.8 GPa phase transition (Rochette et al., 2003). Curves for nickel iron-bearing meteorites have both concave and convex shapes and those for hematite-bearing samples have mostly concave or linear shapes (with average α=1.4).

For iron a high pressure ferromagnetic to paramagnetic phase transition is known to take place at 13 GPa (e.g., Dickinson and Wasilewski, 2000): at this pressure point α-iron (body-centered cubic structure) is transformed into ε-iron (hexagonal close packed structure), which is known to be non-magnetic. In our study pressure demagnetization curve for the sample of synthetic iron has strongly concave shape; furthermore the sample has already lost up to 83% of its initial SIRM under 1.24 GPa. Therefore, an iron sample will most likely lose 100% of its magnetic remanence far below 13 GPa without undergoing any magnetic phase transition.

4. Discussion

In order to check the effect of repeated load (to the same pressure level) on the magnetic remanence, several cycles from 0 to 1.24 GPa were carried out on some of investigated sample

(see Fig. 8). Throughout repeated loads the remanent magnetization under pressure (Fig. 8a) or upon pressure release (Fig. 8b) always shows a slight decrease as a function of number of cycles, consistent with previous works (e.g., Pozzi, 1975; Gilder et al., 2006; Bezaeva et al., 2007). This is not linked to a longer application of maximum pressure as it was shown above (see 3.1) that hydrostatic pressure demagnetization effect is time-independent.

Contrary to the repeated application of the same pressure demagnetization step, repeated application of the same alternating field demagnetization step does not produce a further demagnetization effect of magnetic remanence. This shows that pressure demagnetization and alternating field demagnetization have different physical nature and can not be directly compared in terms of process. Samples that have similar alternating field demagnetization behavior of SIRM can have very different pressure demagnetization behavior (e.g., samples *spi3301* and *bb*, see Fig. 4d, 4j; or samples *bf3201* and *es*t, see Fig. 4e, 4k). Therefore, it is not possible to link a certain pressure value to AF value giving the same degree of demagnetization. AF demagnetizes all grains with coercitivities under a given value whereas pressure demagnetizes grains within a large spectrum of coercivities. Moreover, the degree of demagnetization can vary over the coercivity spectrum of a sample (Gattacceca et al., 2007a).

To represent how pressure demagnetization affects different coercivity fractions of the IRM, we introduced in Bezaeva et al. (2007) the demagnetization loss ε:

$$\varepsilon(B)=[IRM_B(B)-IRM_{BP}(B)]/IRM_B(B), \quad (2)$$

as a function of alternating field B (in mT). IRM_B and IRM_{BP} correspond to IRM values before and after pressure application, respectively, so that $IRM_B(B)$ is a curve of AF demagnetization of initial SIRM and $IRM_{BP}(B)$ is a curve of AF demagnetization of residual IRM after decompression from 1.24 GPa (IRM_{PR}). Curves of $\varepsilon(B)$ for Martian meteorites (*NWA 1068*, *NWA 998*, *LA*), basalt *ba* and rhyolite *rb7a* were presented in Bezaeva et al. (2007, Fig. 3). Table 2 gives (in %) the values of $\varepsilon_1=1-\varepsilon(B=30\text{ mT})/\varepsilon(B=0\text{ mT})$, characterizing the shape of $\varepsilon(B)$ curves. $\varepsilon_1=0$ ($\varepsilon_1=1$) if demagnetization affects only grains with coercivity below (above) 30 mT. In all

cases ε decreases with increasing AF, indicating that pressure preferentially demagnetizes the lower coercivity fractions (consistent with previous works, e.g., Pearce and Karson, 1981) but in some cases high coercivity fractions may also be affected. As seen from Table 2, the average ε_1 value for hematite-bearing samples is of (9±4)%, so mostly low coercivity fractions are affected by pressure demagnetization. For magnetite and titanomagnetite families high coercivity fractions (above 30 mT) are also affected: the average ε_1 is of (69±27)% for magnetites and (69±10)% for titanomagnetites. For pyrrhotite- and nickel iron-bearing samples average ε_1 is of (54±23)% and (53±29)%, respectively.

In most experiments pressure release resulted in further changes of the residual magnetic remanence comparing to the under-pressure level (1.24 GPa). Relative changes in magnetic remanence upon decompression (δ in %) are presented in Table 2. Different magnetic mineralogies have different response to decompression resulting in either further increase (positive δ) of or further decrease (negative δ) in residual remanence (or, more rarely, no changes). An increase of residual IRM upon decompression was observed for pyrrhotite-bearing samples ($1<\delta<8\%$) and hematite-bearing samples ($0<\delta<9\%$). No significant effect was observed on metal, except for the sample of synthetic iron that shows 6% decrease in IRM after pressure release. Ti-rich and Ti-poor(free) magnetites seem to have different behavior of magnetic remanence upon decompression, so they were separated into two groups. Changes in magnetic remanence for Ti-free and Ti-poor magnetites (with $0.03\leq x\leq 0.09$) are in the range -7 to +6%; mostly decrease or negligible increase in remanence are observed apart for synthetic magnetites and *osb10b* sample. Titanomagnetites with high ulvospinel content ($x>0.4$) have generally higher δ (in the 2 to 19% range). Remarkably high δ values are observed for *ba* and *kil-2* samples (13% and 19% recovery of magnetic remanence upon pressure release, respectively). It is interesting to note that both samples are characterized by the highest values of ulvospinel content between all investigated titanomagnetite-bearing samples.

The question of a key parameter that may be responsible for the pressure resistance of different materials has already been put forward in previous works (Pearce and Karson, 1981; Kletetschka et al., 2004). Pearce and Karson (1981) proposed a simple correlation between coercivity and the effect of pressure demagnetization. Kletetschka et al. (2004) suggested that the efficiency of pressure demagnetization is proportional to the logarithm magnetic coercivity (B_c), irrespective of magnetic mineralogy.

We have already shown that the pressure resistance of samples is tightly controlled by their magnetic mineralogy (see above). By analyzing our experimental data, we concluded that for a given magnetic mineralogy, the key proxy for sensitivity of samples to hydrostatic pressure demagnetization is B_{cr} rather than B_c. Indeed, for each magnetic mineralogy pressure resistance is roughly proportional to $\ln(B_{cr})$ (Fig. 9). Synthetic samples of magnetite and iron were not considered for this approximation; synthetic samples of hematite were taken into consideration due to natural provenance of the used hematite powder (natural ore) (Fig. 9). Residual IRM under pressure p_1=0.46 GPa or p_2=1.24 GPa, normalized to initial SIRM (IRM_p), has been fitted using the following equation:

$$IRM_{px}/\mathrm{SIRM} = a_x \cdot \ln(B_{cr}) + b_x, \quad (3)$$

where x=1 for p_1 and x=2 for p_2; a_x and b_x coefficients as well as linear correlation coefficients r_x between IRM_{px}/SIRM and B_{cr} (in mT) are given in Table 3. Strictly speaking B_{cr} value should be dimensionless to equilibrate the equation (as the left part of the equation is dimensionless); this can be easily reached by normalizing the B_{cr} value to 1 mT. Linear correlation coefficients r_x^* between IRM_{px}/SIRM and B_c (in mT) are also given in Table 3. Thus, based on the relative values of r_x and r_x^* (see Table 3), B_{cr} appears to be a better proxy than B_c for all investigated magnetic mineralogies: hematite, pyrrhotite, nickel iron, Ti-magnetite and magnetite, and both pressure values (p_1 and p_2). This could be expected as magnetic remanence should be more directly related to remanent rather than induced properties.

Coefficients of determination or *R*-squared values (R^2_x) reflecting the confidence of a chosen approximation were calculated for logarithmic (3) and linear approximations IRM_{px}/SIRM=$f(B_{cr})$. It was shown that R^2_x was always higher for logarithmic than for linear approximation (except for pyrrhotite under p_1, where both logarithmic and linear approximations have very low R-squared values).

The highest scatter is observed for magnetite and titanomagnetite-bearing samples (Fig. 9d), pointing to a complex behaviour of magnetic remanence versus pressure for this magnetic mineralogy. In Fig. 10 IRM_{p2}/SIRM is plotted versus M_{rs}/M_s for all natural magnetite- and titanomagnetite-bearing samples. M_{rs} and M_s are saturation remanent and induced magnetizations, respectively. As shown in Fig. 10, pressure demagnetization of (Ti-)magnetites is controlled by both ulvospinel content (vertical shift of points on the graph) and magnetic domain structure (horizontal shift of points on the graph). Three sample groups can be delineated: samples with $x \in [0; 0.1]$ (a); samples with $x \in [0.40; 0.55]$ (b) and samples with $x \geq 0.55$ (c). The last group is represented by only two samples (*LA* and *kil-2*). Samples from the three groups lie along three separate trends. As it is seen from Fig. 10, pressure demagnetization efficiency of magnetites and Ti-magnetites is clearly grain-size dependent and increases with increasing grain size (decreasing M_{rs}/M_s). Pressure demagnetization degree of MD magnetites in our study is consistent with the results of Gilder et al. (2006), who showed that MD magnetite retained 66% of its initial SIRM under 1.40 GPa. We did not investigate Ti-free SD magnetite samples that would have allowed confirmation of the surprising result by Gilder et al. (2006) that SD magnetite is more pressure sensitive than MD magnetite despite its higher B_{cr}.

Metal and Ti-free magnetite have the highest intrinsic pressure resistivity (after goethite), but become much more pressure sensitive in their multidomain state. A synthetic graph for all magnetic mineralogies under p_2=1.24 GPa is presented in Fig. 11. The B_{cr} value corresponding to the threshold, above which no further pressure demagnetization could be produced under 1.24 GPa (called B_{th}), was determined for each magnetic mineralogy (Table 3). The highest value of

B_{th} corresponds to hematite, which appears to be the most pressure sensitive material in agreement with the lowest MDS values found for hematite-bearing samples. Based on other B_{th} values, magnetite and Ti-magnetite appear as pressure sensitive as nickel iron but more pressure resistant than pyrrhotite (in the coercivity window B_{cr}>33 mT). Goethite was found to be the most pressure resistant mineral. Based on the two greigite samples, this mineral appears to be more sensitive to pressure than magnetite.

5. Conclusions

This study gives an overview of the sensitivity to pressure demagnetization (by a purely hydrostatic load up to 1.24 GPa) of geological and extraterrestrial materials as well as synthetic samples with a variety of magnetic mineralogies: magnetite and titanomagnetite, pyrrhotite, greigite, hematite, goethite as well as iron and iron-nickel alloys. Magnetic remanence under pressure and upon decompression was investigated using a non-magnetic high pressure cell of piston-cylinder type together with a high sensitivity remanence magnetometer (SQUID magnetometer).

After showing the good reproducibility of our experiments, we demonstrated the additivity of partial pressure demagnetization. It was found that under hydrostatic pressure of 1.24 GPa, applied in a low magnetic field (<5 μT), rock and synthetic samples lost irreversibly up to 84% of their initial saturation isothermal remanent magnetization without any changes in their intrinsic magnetic properties. Decompression resulted in further changes in IRM (decrease or increase up to 19% with respect to the initial SIRM value before compression) but decompressed residual IRM never reached SIRM value before compression.

It was shown that hydrostatic pressure demagnetization is not time-dependent, but repeated application of the same pressure level leads to further demagnetization. The main factor controlling the stability of remanent magnetization versus hydrostatic pressure is magnetic mineralogy. For a given magnetic mineralogy the resistance to pressure is roughly proportional

to ln(B_{cr}), where B_{cr} is the coercivity of remanence (reflecting the magnetic hardness of the sample).

Thus, based on our experimental investigations, we propose a phenomenological model allowing to quantify the pressure demagnetization effect (Fig. 11, Table 3): after identification of the main magnetic mineralogy of the sample and by measuring its B_{cr} value, it is possible to roughly estimate the resistance of its magnetic remanence to a purely hydrostatic load of 0.46 and 1.24 GPa. For magnetite and titanomagnetite such a model must be refined by considering the magnetic domain state and the substitution rate x (Fig. 10). The pressure demagnetization effect was shown to be grain-size sensitive: the efficiency of pressure demagnetization typically increases with increasing grain size.

Acknowledgements

This work was supported by the French Agence Nationale de la Recherche (project 05-JCJC-0133) and was partially funded by the CNRS-RFFI PICS program (grant №07-05-92165) while the stay of N.S. Bezaeva at CEREGE was funded by a research grant of the French Government (№2005814). We acknowledge K.L. Louzada (Harvard University, Cambridge, USA) for providing basalt samples from the Lonar crater (PD6-2-1, PD6-2-4). C. Francis (Harvard Museum of Natural History, Cambridge, USA) is acknowledged for providing the pyrrhottite samples 98080 and 127037. We are grateful to B. Zanda (Museum National d'Histoire Naturelle, Paris, France) and M.A. Nazarov (Vernadsky Institute for Geochemistry and Analytical Chemistry RAS, Moscow, Russia) for providing some meteorite samples. We thank A.P. Roberts (University of Southampton, Southampton, UK) and A.R. Muxworthy (Imperial College of London, London, UK) for providing greigite samples.

References

Avchyan, G.M., 1967. Effect of hydrostatic pressure up to 8000 kg/cm^2 on various types of remanent magnetization of rocks (translated from Russian). Izv. Phys. Solid Earth, 7: 465-469.

Bezaeva, N.S., Rochette, P., Gattacceca, J., Sadykov, R.A., Trukhin, V.I., 2007. Pressure demagnetization of the Martian crust: Ground truth from SNC meteorites. Geophys. Res. Lett., 34: L23202, doi: 10.1029/2007GL031501.

Chen, G., Ahrens, T.J., Hide, R., 1995. Hypervelocity impacts and magnetization of small bodies in the solar system. Icarus, 115: 86-96.

Cisowski, S.M., Dunn, J.R., Fuller, M., YeeMing, Wu., 1976. Magnetic effects of shock and their implications for lunar magnetism (II). In: Proc. Lunar Sci. Conf. 7th: 3299-3320.

Cisowski, S.M., Fuller, M., 1978. The effect of shock on the magnetism of terrestrial rocks. J. Geophys. Res., 83: 3441-3458.

Dekkers, M.J., 1988. Magnetic properties of natural pyrrhotite part 1: Behavior of initial susceptibility and saturation-magnetization related parameters in a grain-size dependent framework. Phys. Earth Planet. Int. 52: 376-393.

Dickinson, T. L., Wasilewski, P., 2000. Shock magnetism in fine particle iron. Meteor. Planet. Sci., 35: 65-74.

Dunlop, D., Özdemir, O., 1997. Rock Magnetism: Fundamentals and Frontiers. Cambridge University Press, Cambridge, 573 pp.

Florindo, F., Sagnotti, L., 1995. Palaeomagnetism and rock magnetism in the upper Pliocene Valle Ricca (Rome, Italy) section. Geophys. J. Int., 123: 340-354.

Gattacceca, J., Rochette, P., Bourot-Denise, M., 2003. Magnetic properties of a freshly fallen LL ordinary chondrite: the Bensour meteorite. Phys. Earth Planet. Int., 140: 343-358.

Gattacceca, J., Orsini, J.-B., Bellot, J.-P., Henry, B., Rochette, P., Rossi, P., Cherchi, G., 2004. Magnetic fabric of granitoids from Southern Corsica and Northern Sardinia and

implications for Late Hercynian tectonic setting. J. Geological Society, London, 161: 277-289.

Gattacceca, J., Boustie, M., Weiss, B., Rochette, P., Lima, E.A., Fong, L.E., Baudenbacher, F.J., 2006. Investigating impact demagnetization through laser impacts and SQUID microscopy. Geology, 34: 333-336, doi: 10.1130/G21898.1.

Gattacceca, J., Lamali, A., Rochette, P., Boustie, M., Berthe, L., 2007a. The effect of explosive-driven shocks on the natural remanent magnetization and the magnetic properties of rocks. Phys. Earth Planet. Int., 162: 85-98.

Gattacceca, J., Deino, A., Rizzo, R., Jones, D.S., Henry, B., Beaudoin, B., Vadeboin, F., 2007b. Miocene rotation of Sardinia: New paleomagnetic and geochronological constraints and geodynamic implications. Earth Planet Sci. Lett., 258: 359-377.

Gattacceca, J., Berthe, L., Boustie, M., Vadeboin, F., Rochette, P., De Resseguier, T., 2008. On the efficiency of shock magnetization processes. Phys. Earth Planet. Int., 166: 1-10.

Gilder, S.A., Le Goff, M., Chevrin, J.-C., 2006. Static stress demagnetization of single and multidomain magnetite with implications to meteorite impacts. High Pressure Research, 26: 539-547.

Gilder, S.A., Le Goff, M., 2008. Systematic pressure enchancement of titanomagnetite magnetization. Geophys. Res. Lett., 35: L10302, doi: 10.1029/2008GL033325.

Halekas, J.S., Mitchell, D.L., Lin, R.P., Hood, L.L., Acuña, M.H., Binder, A.B., 2002. Demagnetization signatures of lunar impact craters. Geophys. Res. Lett., 29: 23-1, doi: 10.1029/2001GL013924.

Halekas, J.S., Lin, R.P., Mitchell, D.L., 2003. Magnetic fields of lunar multi-ring impact basins. Meteor. Planet. Sci., 38: 565-578.

Halls, H.C., 1979. The State of Islands meteorite impact site: a study of shock remanent magnetization. Geophys. J. R. Astr. Soc., 59: 553-591.

568 Hargraves, R.B., Perkins, W.E., 1969. Investigations of the effect of shock on natural remanent
569 magnetism. J. Geophys. Res., 74: 2576-2589.
570 Hood, L., Richmond, N.C., Pierazzo, E., Rochette, P., 2003. Distribution of crustal magnetic
571 fields on Mars: shock effects of basin-forming impacts. Geophys. Res. Lett., 30: doi:
572 10.1029/2002GL016657.
573 Hood, L.L., Harrison, K.P., Langlais, B., Lillis, R.J., Poulet, F., and Williams, D.A. 2009.
574 Magnetic anomalies near Apollinaris Patera and the Medusae Fossae Formation in Lucus
575 Planum, Mars. Icarus (submitted).
576 Hornemann, U., Pohl J., Bleil, U., 1975. A compressed air gun accelerator for shock
577 magnetization and demagnetization experiments up to 20 kbar. J. Geophys., 41: 13-22.
578 Horng, C.-S., Torii, M., Shea, K.-S., Kao, S.-J., 1998. Inconsistent magnetic polarities between
579 greigite- and pyrrhotite/ magnetite-bearing marine sediments from the Tsailiao-chi
580 section, southwestern Taiwan. Earth Planet. Sci. Lett., 164: 467-481.
581 Hunt, C.P., Moskowitz, B.M., Banerjee, S.K., 1995. Magnetic properties of rocks and minerals.
582 In: T.J. Ahrens (Editor). Rock Physics and Phase Relations: A Handbook of Physical
583 Constants, Am. Geophys. Union, Reference Shelf 3: 189-204.
584 Jiang, W.-T., Horng, C.-S., Roberts, A.P., Peacor, D.R., 2001. Contradictory magnetic polarities
585 in sediments and variable timing of neoformation of authigenic greigite. Earth Planet.
586 Sci. Lett., 193: 1-12.
587 Kinoshita, H., 1968. Studies on Piezo-Magnetization (III) PRM and Relating Phenomena. J.
588 Geomag. Geoelectr., 20: 155-167.
589 Kirichenko, A.S., Kornilov, A.V., Pudalov, V.M., 2005. Properties of polyethilsiloxane as a
590 pressure-transmitting medium. Instr. Experim. Tech., 48(6): 813-816, doi:
591 10.1007/s10786-005-0144-5 (translated from Russian).
592 Kletetschka, G., Connerney, J.E.P., Ness, N.F., Acuña, M.H., 2004. Pressure effects on Martian
593 crustal magnetization near large impact basins. Meteorit. Planet. Sci., 39: 1839-1848.

Louzada, K.L., Stewart, S.T., Weiss, B.P., 2007. Effect of shock on the magnetic properties of pyrrhotite, the Martian crust and meteorites. Geophys. Res. Lett., 34: L05204, doi: 10.1029/2006GL027685.

Louzada, K.L., Weiss, B.P., Maloof, A.C., Stewart, S.T., Swanson-Hysell, N.L., Soule, S.A., 2008. Paleomagnetism of Lonar impact crater, India. Earth Planet. Sci. Lett., 275: 308-319.

Louzada, K.L., Stewart, S.T., Weiss, B.P., Gattacceca, J., Bezaeva, N.S., 2009. Shock and Static Pressure Demagnetization of Pyrrhotite and Implications for the Martian Crust. Earth Planet. Sci. Lett. (accepted).

Martelli, G., Newton, G., 1977. Hypervelocity cratering and impact magnetization of basalt. Nature, 269: 478-480.

Martin, R.J., Noel, J.S., 1988. The influence of stress path on thermoremanent magnetization. Geophys. Res. Lett., 15: 507-510.

Nagata, T., 1966. Main characteristics of piezo-magnetization and their qualitative interpretation. J. Geomag. Geoelectr., 18: 81-97.

Nishioka, I., Funaki, M., Toshimori, S., 2007. Shock-induced anisotropy of magnetic susceptibility: impact experiment on basaltic andesite. Earth Planets Space, 59: e45–e48.

Pearce, G.W., Karson, J.A., 1981. On pressure demagnetization. Geophys. Res. Lett. 8: 725-728.

Pesonen, L.J., Marcos, N., Pipping, F., 1992. Palaeomagnetism of the Lappajärvi impact structure, western Finland, 216: 123-142.

Pesonen, L.J., Deutsch, A., Hornemann, U., Langenhorst, F., 1997. Magnetic properties of diabase samples shocked experimentally in the 4.5 to 35 GPa range. In: Proc. Lunar Planet. Sci. Conf. 28th: 1087-1088.

Pilkington, M., Grieve, R.A.F., 1992. The geophysical signature of terrestrial impact craters. Rev. Geophys., 30: 161-181.

619 Pohl J., Bleil U., Hornemann U. 1975. Shock magnetization and demagnetization of basalt by
620 transient stress up to 10 kbar. J. Geophys. 41: 23-41.
621 Pozzi, J.P., 1973. Effets de pression en magnétisme des roches, Ph.D Thesis, Université Paris VI,
622 Paris, France.
623 Pozzi, J.P., 1975. Magnetic properties of oceanic basalts – effects of pressure and consequences
624 for the interpretation of anomalies. Earth Planet. Sci. Lett., 26: 337-344.
625 Rochette, P., Bertrand, H., Braun, C., Berger, E., 1993. La province volcanique Pléistocène
626 supérieur du Bas-Vivarais (Ardèche, France): propagation de fentes crustales en
627 échelons? C.R. Acad. Sci. Paris, 316: 913-920.
628 Rochette, P., Tamrat, E., Féraud, G., Pik, R., Courtillot, V., Ketefo, E., Coulon, C., Hoffmann,
629 C., Vandamme, D., Yirgu, G., 1998. Magnetostratigraphy and timing of the Oligocene
630 Ethiopian traps. Earth Planet. Sci. Lett., 164: 497-510.
631 Rochette, P., Lorand, J.-P., Fillion, G., Sautter, V., 2001. Pyrrhotite and the remanent
632 magnetization of SNC meteorites: a changing perspective on Martian magnetism. Earth
633 Planet. Sci. Lett., 190: 1-12.
634 Rochette, P., Fillion, G., Ballou, R., Brunet, F., Ouladdiaf, B., Hood, L., 2003. High pressure
635 magnetic transition in pyrrhotite and impact demagnetization on Mars. Geophys. Res.
636 Lett. 30: 1683, doi: 10.1029/2003GL017359.
637 Rochette, P., Gattacceca, J., Chevrier, V., Hoffmann, V., Lorand, J.-P., Funaki, M., Hochleitner,
638 R., 2005a. Matching Martian crustal magnetization and magnetic properties of Martian
639 meteorites. Meteor. Planet. Sci., 40: 529-540.
640 Rochette, P., Mathe, P.-E., Esteban, L., Rakoto, H., Bouchez, J.-L., Liu, Q., Torrent, J., 2005b.
641 Non-saturation of the defect moment of goethite and fine-grained hematite up to 57
642 Teslas. Geophys. Res. Lett., 32: L22309, doi: 10.1029/2005GL024196.
643 Rochette, P., Gattacceca, J., Bonal, L., Bourot-Denise, M., Chevrier, V., Clerc, J.-P.,
644 Consolmagno, G., Folco, L., Gounelle, M., Kohout, T., Pesonen, L., Quirico, E.,

Sagnotti, L., Skripnik, A., 2008. Magnetic Classification of Stony Meteorites: 2. Non-Ordinary Chondrites. Meteor. Planet. Sci., 43: 959-980.

Sadykov, R.A., Bezaeva, N.S., Kharkovskiy, A.I., Rochette, P., Gattacceca, J., Trukhin, V.I., 2008. Nonmagnetic high pressure cell for magnetic remanence measurements up to 1.5 GPa in a superconducting quantum interference device magnetometer. Rev. Sci. Instr., 79: 115102, doi: 10.1063/1.2999578.

Srnka, L.J., Martelli, G., Newton, G., Cisowski, S.M., Fuller, M.D., Schaal, R.B., 1979. Magnetic field and shock effects and remanent magnetization in a hypervelocity impact experiments. Earth Planet. Sci. Lett., 42: 127-137.

Valeev, K.A., 1984. Magnetic properties of rocks at high pressures and temperatures and the problem of magnetoactive layer of the Earth's crust and upper mantle. Thesis for a Doctor's degree, M.V. Lomonosov Moscow State University, Moscow, Russia (in Russian).

Van Dongen, B.E., Roberts, A.P., Schouten, S., Jiang, W-T., Florindo, F., Pancost, R.D., 2007. Formation of iron sulfide nodules during anaerobic oxidation of methane. Geochim. Cosmochim. Acta, 71: 5155–5167

Vlag, P., Vandamme, D., Rochette, P., Spinelli, K., 1997. Paleomagetism in the Esterel rocks: a revisit 22 years after the thesis of H. Zijderveld. Geologie en Mijnbouw, 76: 21-33.

Figure captions:

Figure 1. Scheme of assembled high pressure cell (cross-sectional view) (a) with manganin pressure sensor (obturator) and (b) without obturator. All cell dimensions are indicated in millimeters. *1*: wires, *2*: pusher, *3*: upper locking screw, *4*: obturator, *5*: antiextrusion gaskets, *6*: manganin sensor (coil), *7*: teflon cavity, *8*: pressure transmitting medium (PES-1), *9*: sample, *10*: fixing teflon spiral, *11*: lower locking screw, *12*: piston support, *13*: inner piston, *14*: inner part in Russian alloy (NiCrAl), *15*: outer part in titanium alloy, *16*: pusher, *17*: piston support, *18*: inner piston, *19*: antiextrusion gasket, *20*: teflon plug. Elements 2, 4, 12–13, and 16-18 are made of Russian alloy while elements 3 and 11 are made of titanium alloy.

Figure 2. Example of correction of the pressure demagnetization curve of hematite-bearing rhyolite (sample *rb7a*) by the magnetic moment of the pressure cell. The lower curves correspond to the cell remanent magnetic moment M_r under pressure versus pressure after 5, 10 and 15 min of relaxation of the cell in a magnetically shielded room. The upper curves correspond to the uncorrected (dashed line) and vectorially corrected (solid line) pressure demagnetization curves (residual IRM under pressure versus pressure) of *rb7a*.

Figure 3. Residual isothermal remanent magnetization under pressure (normalized to initial SIRM) versus pressure for two subsamples of radiolarite (*radiol-1* and *radiol-2*), originated from the same initial sample; two subsamples of Bensour meteorite (*Bensour-i* and *Bensour-j*); synthetic sample of magnetite powder set into epoxy resin (*magn6c*). Pressure experiments on *magn6c* sample were carried out twice in order to check for the reproducibility of the pressure demagnetization effect (curves *magn6a (1)* and *magn6c (2)*, respectively).

689 **Figure 4** (**a-f):** Residual isothermal remanent magnetization under pressure (normalized to initial
690 SIRM) versus pressure. Each curve corresponds to a different sample. **(g-l):** Alternating field
691 (AF) demagnetization of normalized SIRM. Pressure demagnetization and AF demagnetization
692 curves corresponding to the same sample are indicated by the same plot style and symbols. a)-g)
693 pyrrhotite- and greigite-bearing samples, b)-h) hematite and goethite-bearing samples, c)-i) iron
694 and nickel iron-bearing samples, d)-j) titanomagnetite-bearing samples, e),f)-k),l) magnetite-
695 bearing samples.
696
697 **Figure 5.** Residual isothermal remanent magnetization under pressure (normalized to initial
698 SIRM) versus pressure for four different microdiorite subsamples, originated from the same
699 initial sample.
700
701 **Figure 6.** Residual remanent magnetization under pressure (normalized to its initial value of
702 NRM, TRM or IRM) versus pressure. Each curve corresponds to a different sample.
703
704 **Figure 7.** Alternating field (AF) demagnetization curves of initial SIRM, residual IRM after
705 decompression from 1.24 GPa and SIRM acquired after decompression for a magnetite-bearing
706 granite sample (*bf9804*). AF demagnetization curves of initial SIRM and SIRM after
707 decompression are indistinguishable.
708
709 **Figure 8.** (a) Residual remanent magnetization under 1.24 GPa versus number of compression
710 cycles up to 1.24 GPa. (b) residual remanent magnetization upon decompression from 1.24 GPa
711 versus number of compression cycles up to 1.24 GPa.
712
713 **Figure 9.** Residual remanent magnetization (normalized to initial SIRM) under p_1=0.46 GPa
714 (open symbols) and p_2=1.24 GPa (solid symbols) versus coercivity of remanence B_{cr} for (a)

715 pyrrhotite-bearing samples; (b) hematite-bearing samples; (c) nickel-iron bearing samples (the
716 sample of synthetic iron is not considered); (d) magnetite- and titanomagnetite-bearing samples
717 (synthetic samples of magnetite are not considered). Logarithmic approximation is indicated for
718 each mineralogy (see also Table 3). The data points indicated by open and solid circles are not
719 taken into account in the logarithmic fit: for nickel iron-bearing samples (c) because of the
720 absence of further demagnetization effect above B_{cr}=70 mT; for magnetite- and titanomagnetite-
721 bearing samples (d) because of a clear outlier of the data point.
722
723 **Figure 10.** Residual remanent magnetization (normalized to initial SIRM) under 1.24 GPa
724 versus M_{rs}/M_s ratio for magnetite- and titanomagnetite-bearing samples with different ulvospinel
725 content. M_{rs} and M_s are saturation remanent and induced magnetizations.
726
727 **Figure. 11.** Synthetic graph of residual remanent magnetizations (normalized to initial SIRM)
728 under 1.24 GPa versus coercivity of remanence B_{cr} for different magnetic mineralogies.
729 Logarithmic fits correspond to the indicated fits by solid lines from Fig. 9.
730

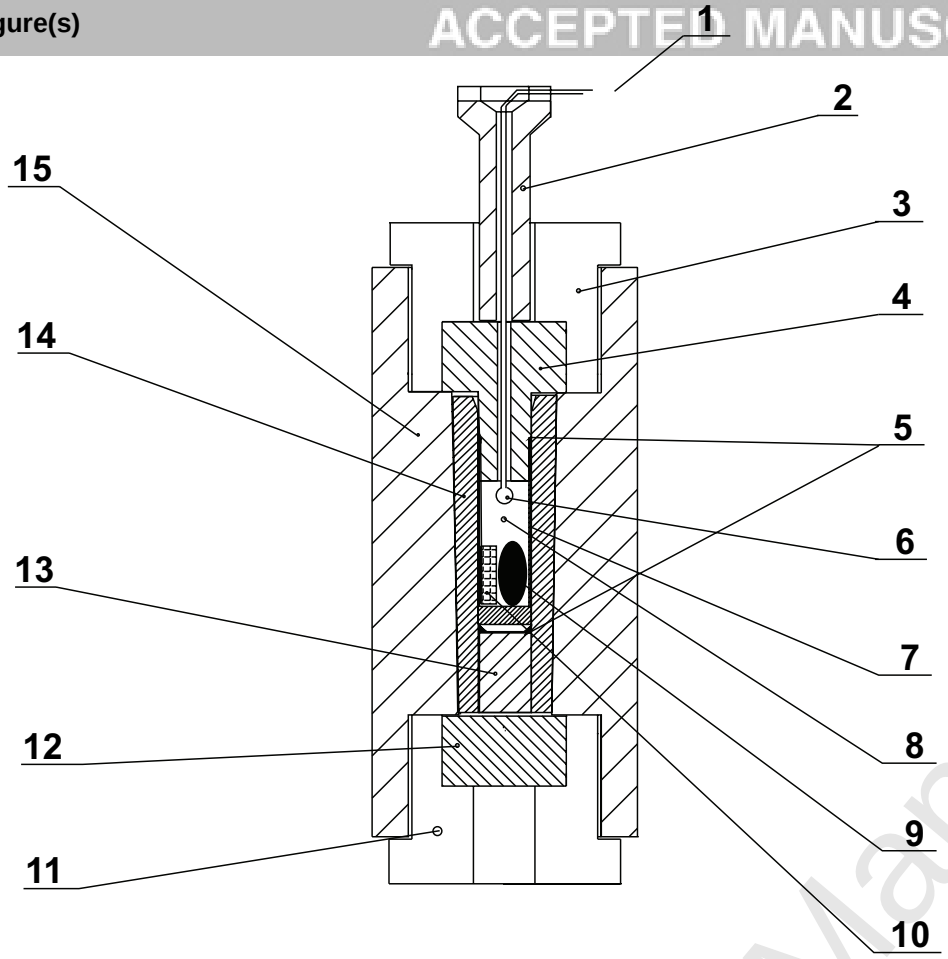

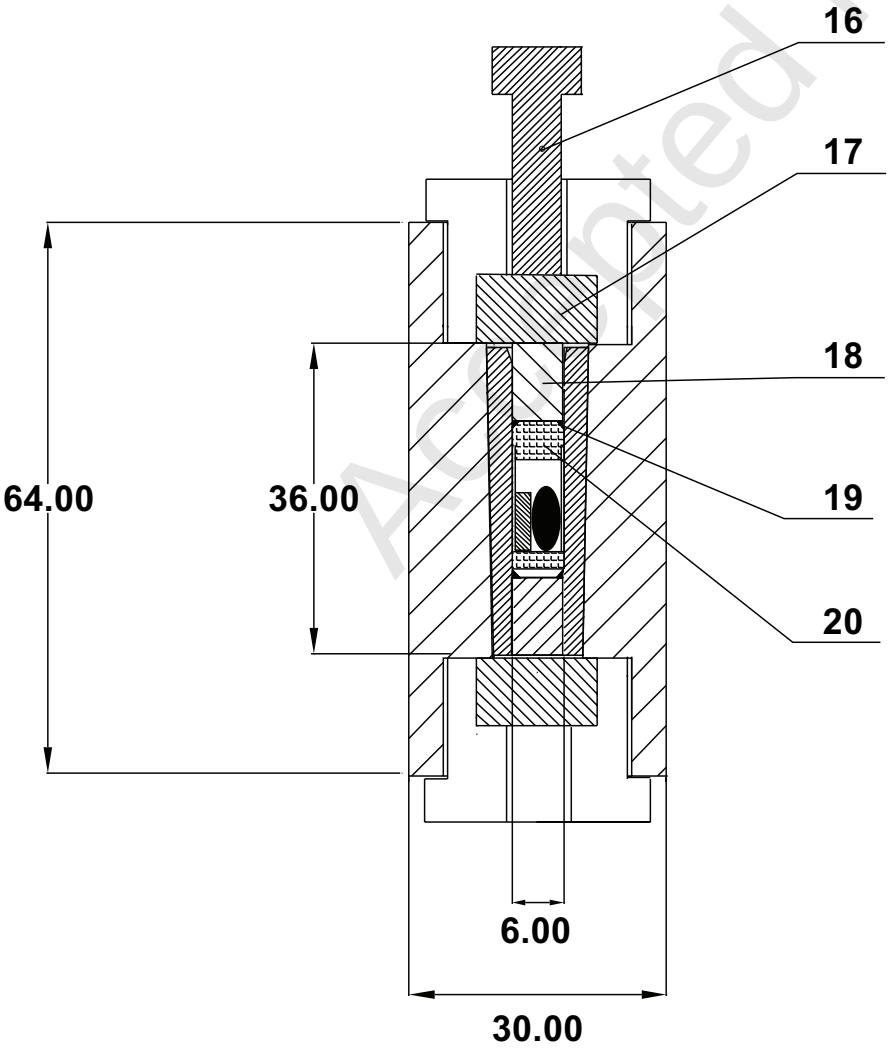

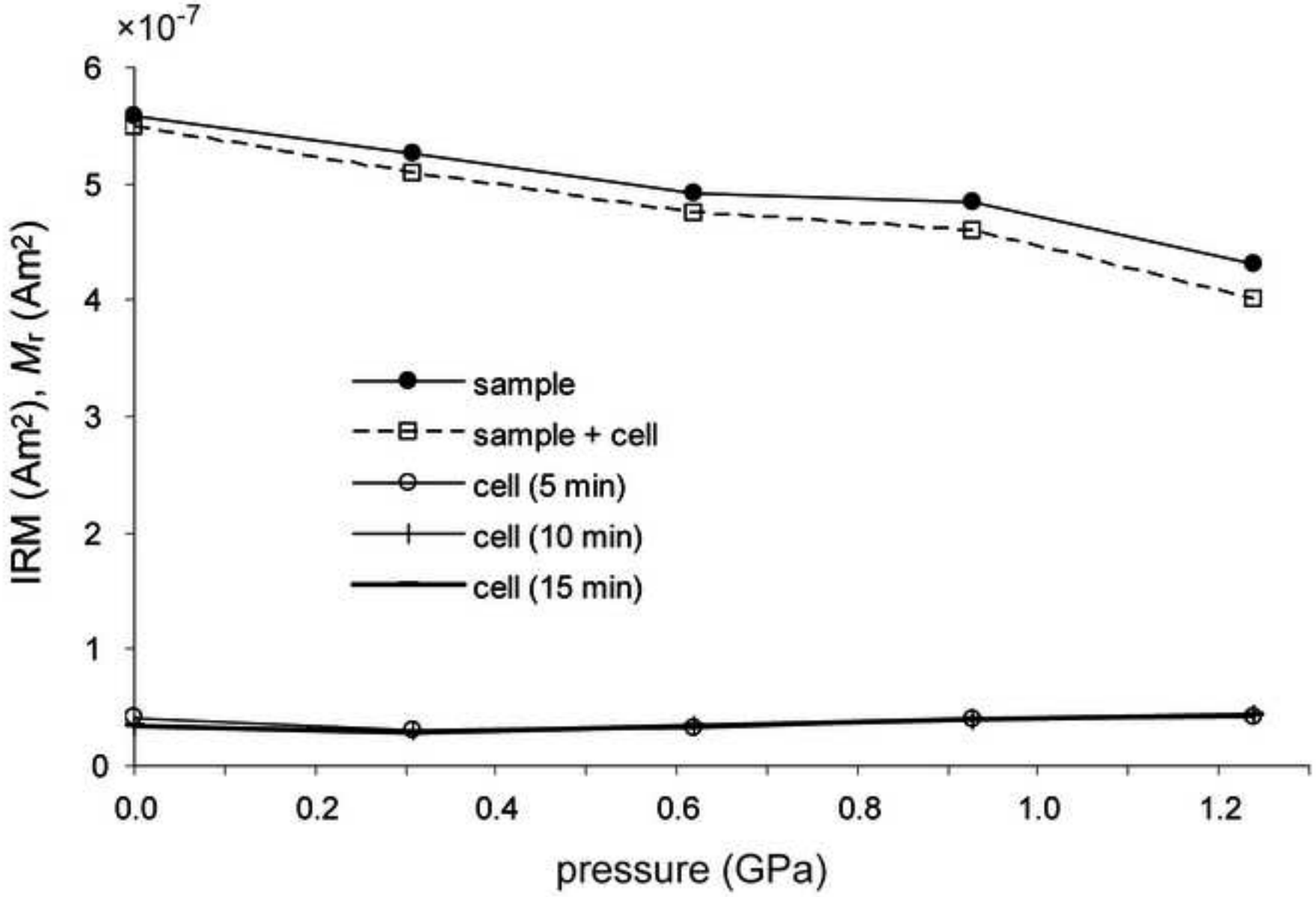
×10-7
6
5
4
3
2
1
0
IRM (Am²), Mr (Am²)
sample
sample + cell
cell (5 min)
cell (10 min)
cell (15 min)
0.0
0.2
0.4
0.6
0.8
1.0
1.2
pressure (GPa)

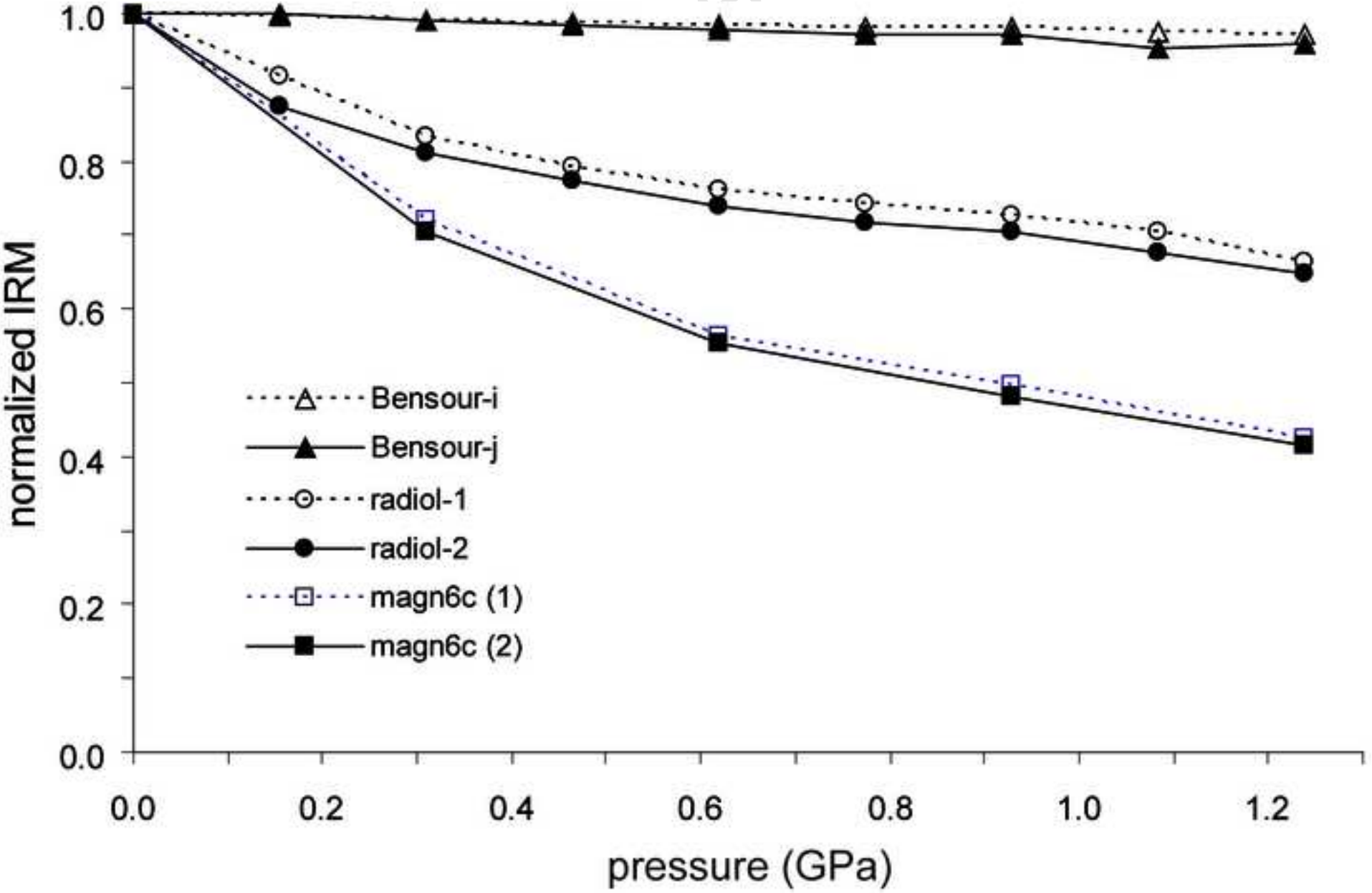
normalized IRM
1.0
0.8
0.6
0.4
0.2
0.0
0.0
0.2
0.4
0.6
0.8
1.0
1.2
pressure (GPa)
Bensour-i
Bensour-j
radiol-1
radiol-2
magn6c (1)
magn6c (2)

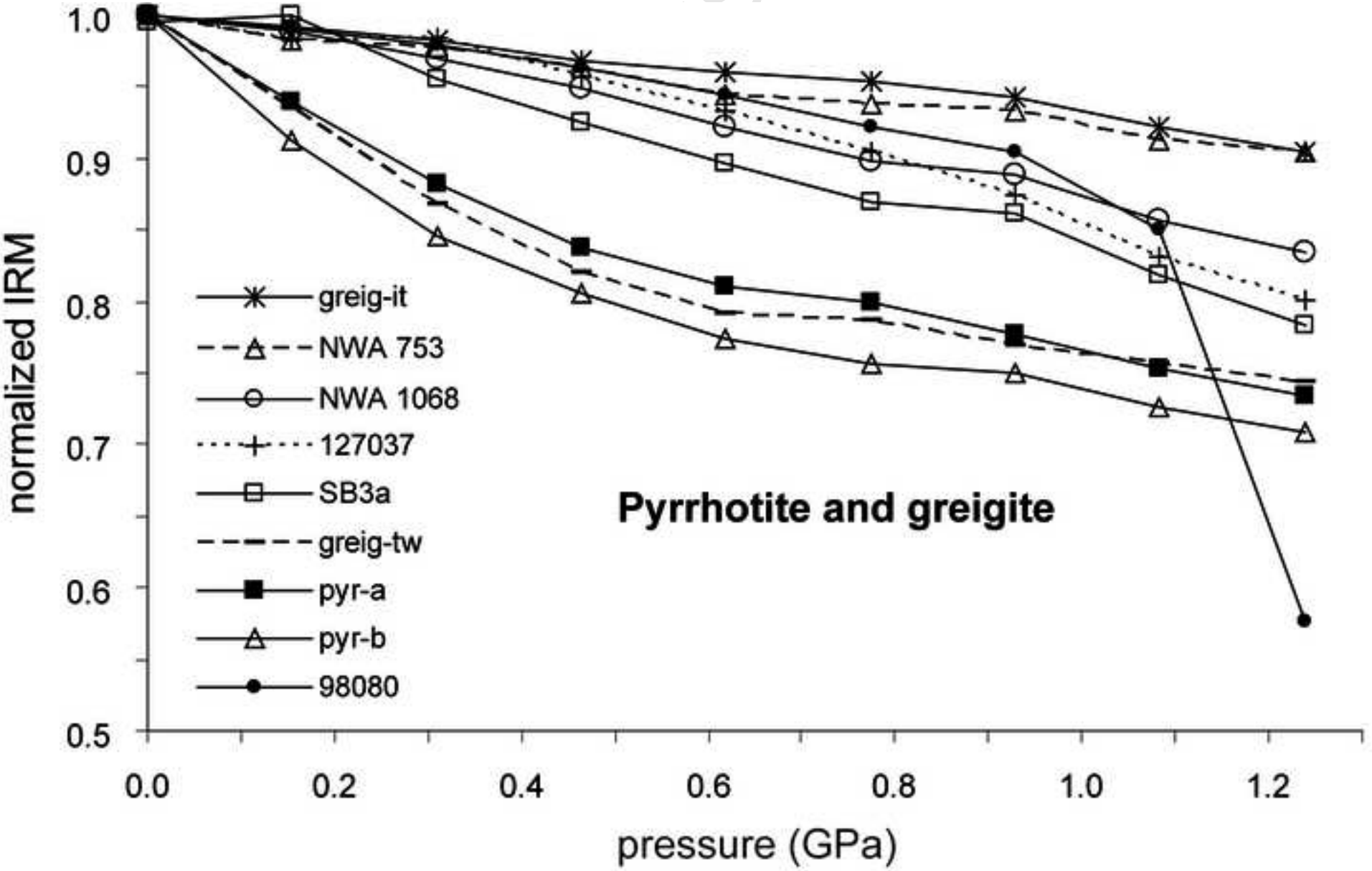
normalized IRM
1.0
0.9
0.8
0.7
0.6
0.5
0.0
0.2
0.4
0.6
0.8
1.0
1.2
pressure (GPa)
greig-it
NWA 753
NWA 1068
127037
SB3a
greig-tw
pyr-a
pyr-b
98080
Pyrrhotite and greigite

Figure(s)

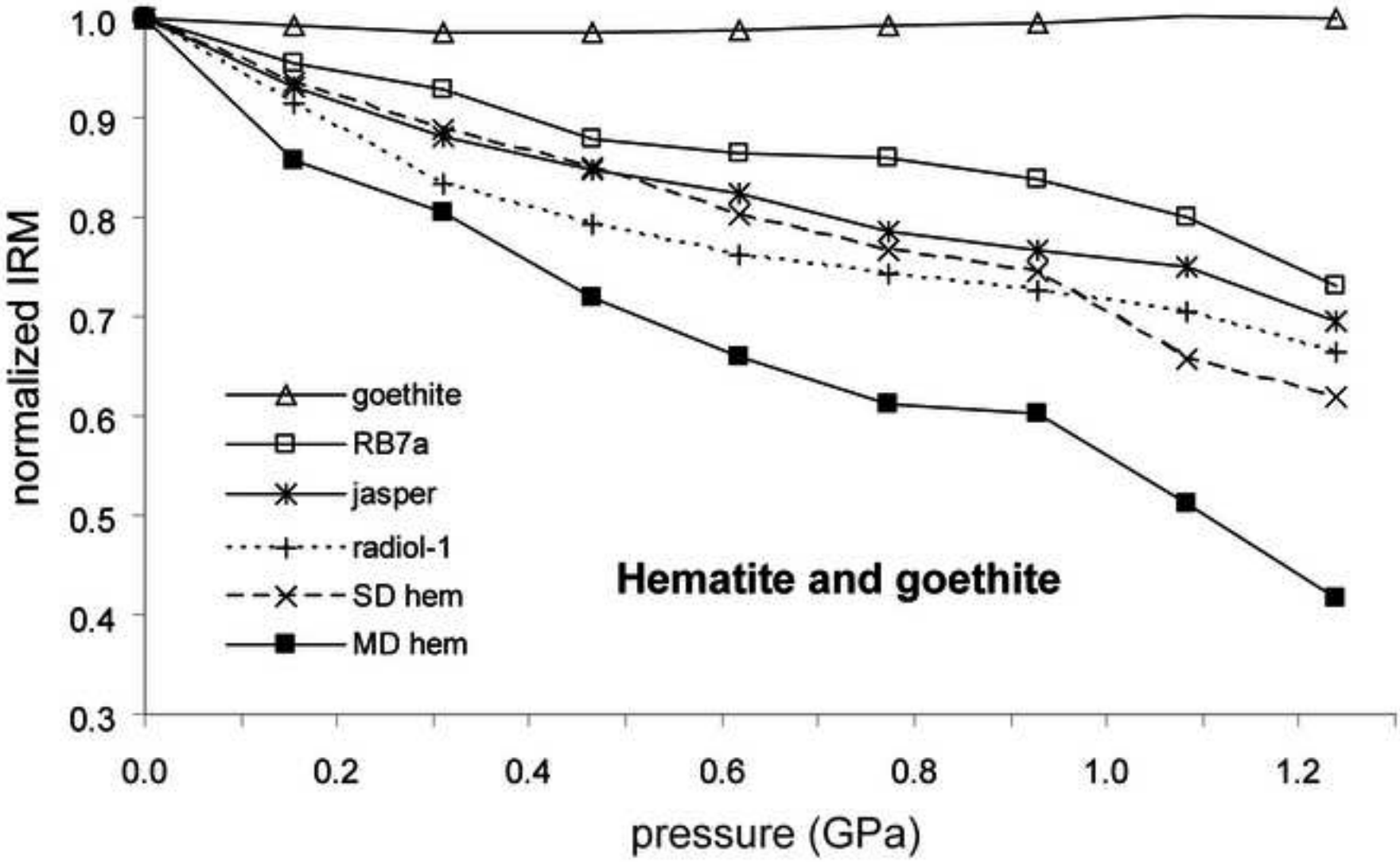
normalized IRM
1.0
0.9
0.8
0.7
0.6
0.5
0.4
0.3
0.0
0.2
0.4
0.6
0.8
1.0
1.2
pressure (GPa)
goethite
RB7a
jasper
radiol-1
SD hem
MD hem
Hematite and goethite

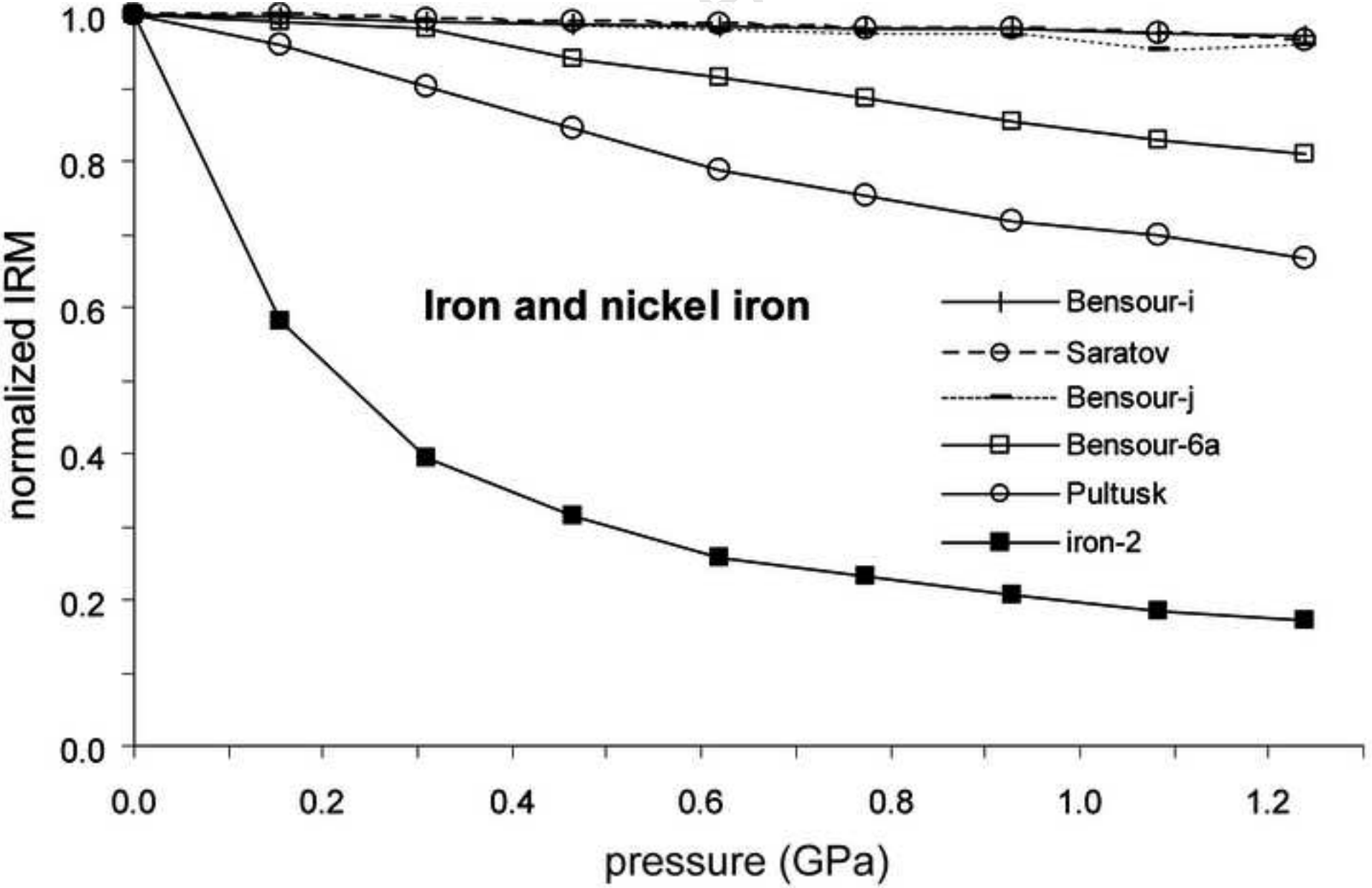
Iron and nickel iron
normalized IRM
pressure (GPa)
1.0
0.8
0.6
0.4
0.2
0.0
0.0
0.2
0.4
0.6
0.8
1.0
1.2
Bensour-i
Saratov
Bensour-j
Bensour-6a
Pultusk
iron-2

Figure(s)

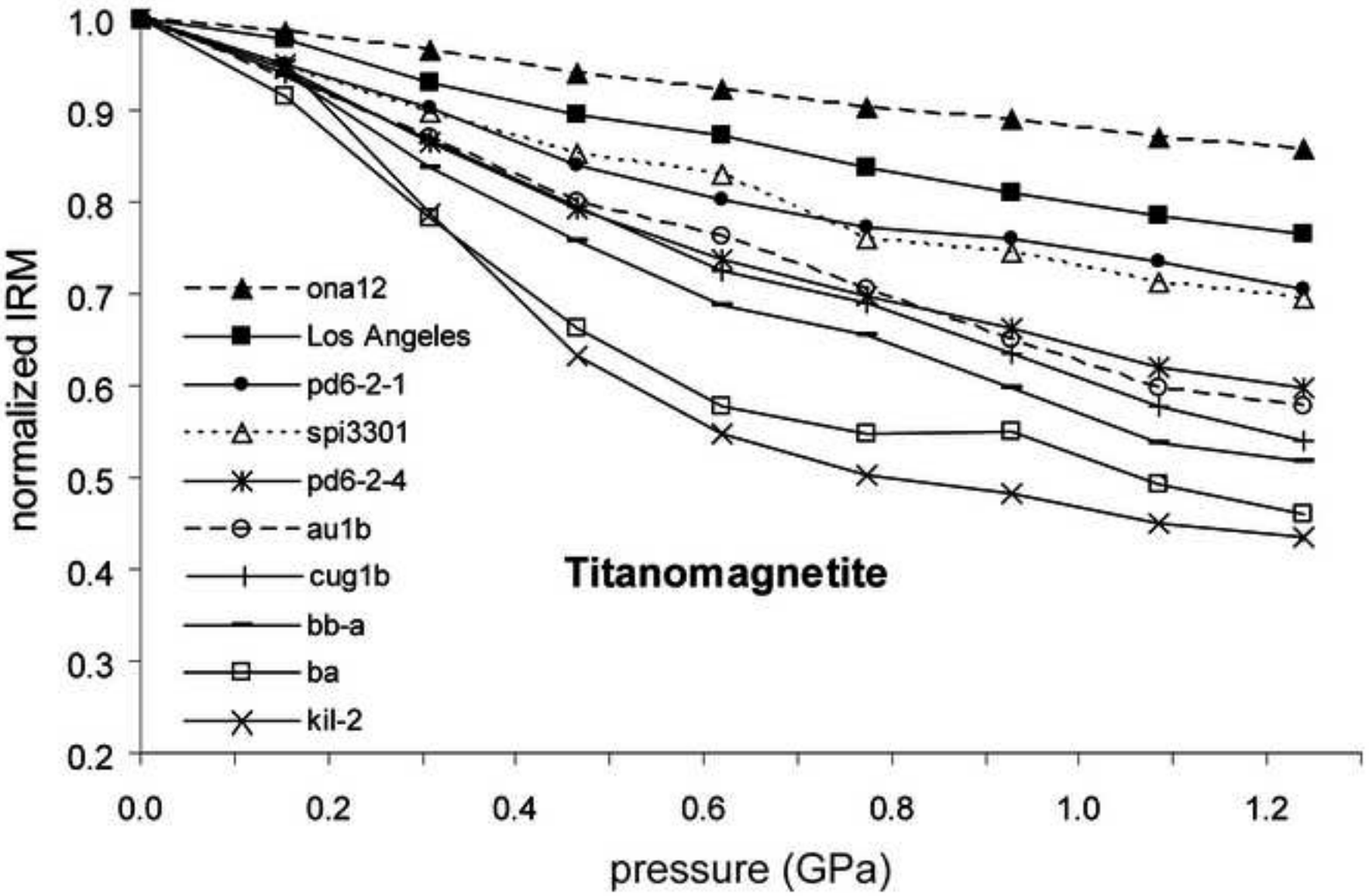
normalized IRM
1.0
0.9
0.8
0.7
0.6
0.5
0.4
0.3
0.2
0.0
0.2
0.4
0.6
0.8
1.0
1.2
pressure (GPa)
ona12
Los Angeles
pd6-2-1
spi3301
pd6-2-4
au1b
cug1b
bb-a
ba
kil-2
Titanomagnetite

Figure(s)

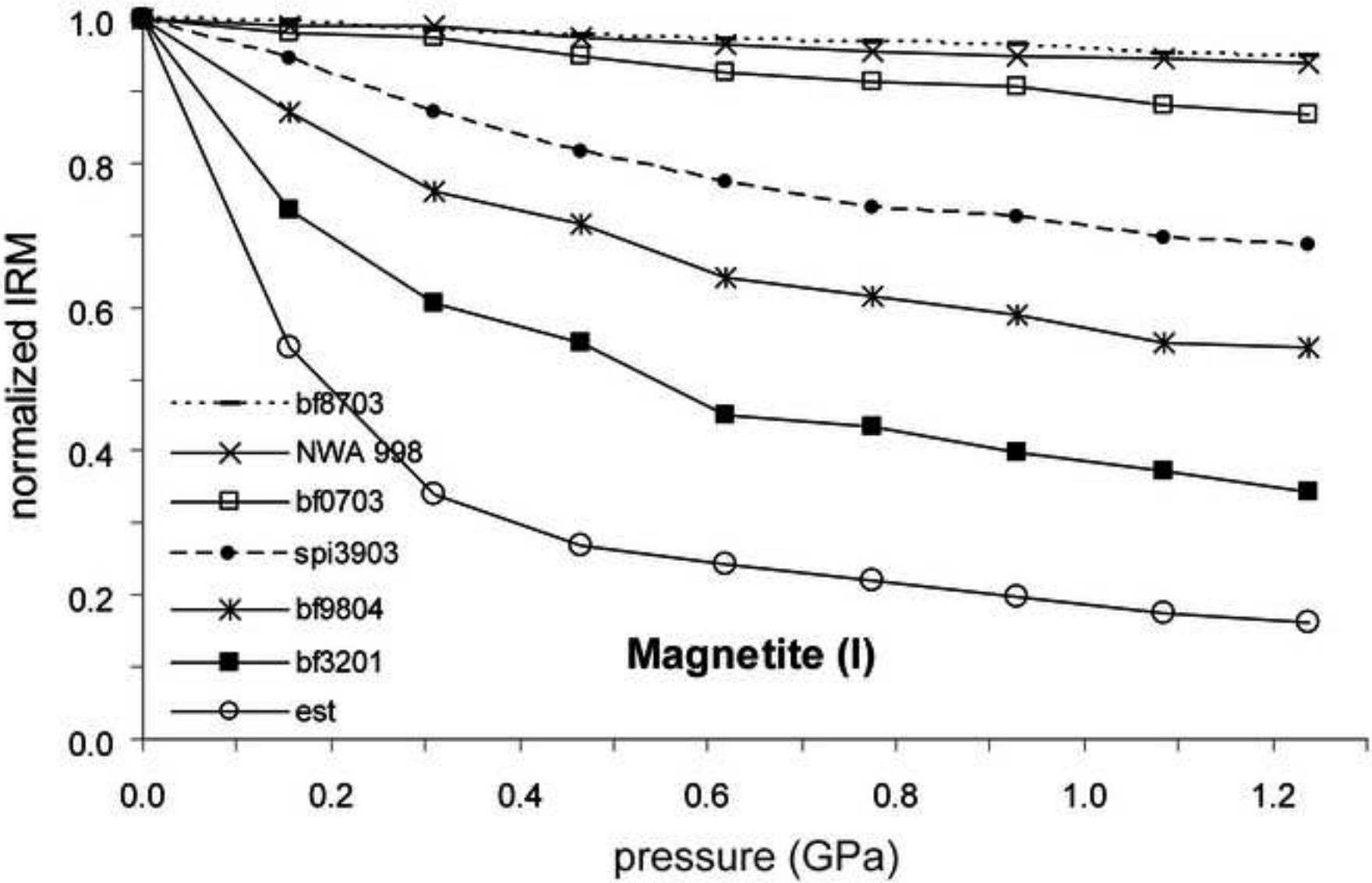
normalized IRM
1.0
0.8
0.6
0.4
0.2
0.0
bf8703
NWA 998
bf0703
spi3903
bf9804
bf3201
est
Magnetite (I)
0.0
0.2
0.4
0.6
0.8
1.0
1.2
pressure (GPa)

Figure(s)

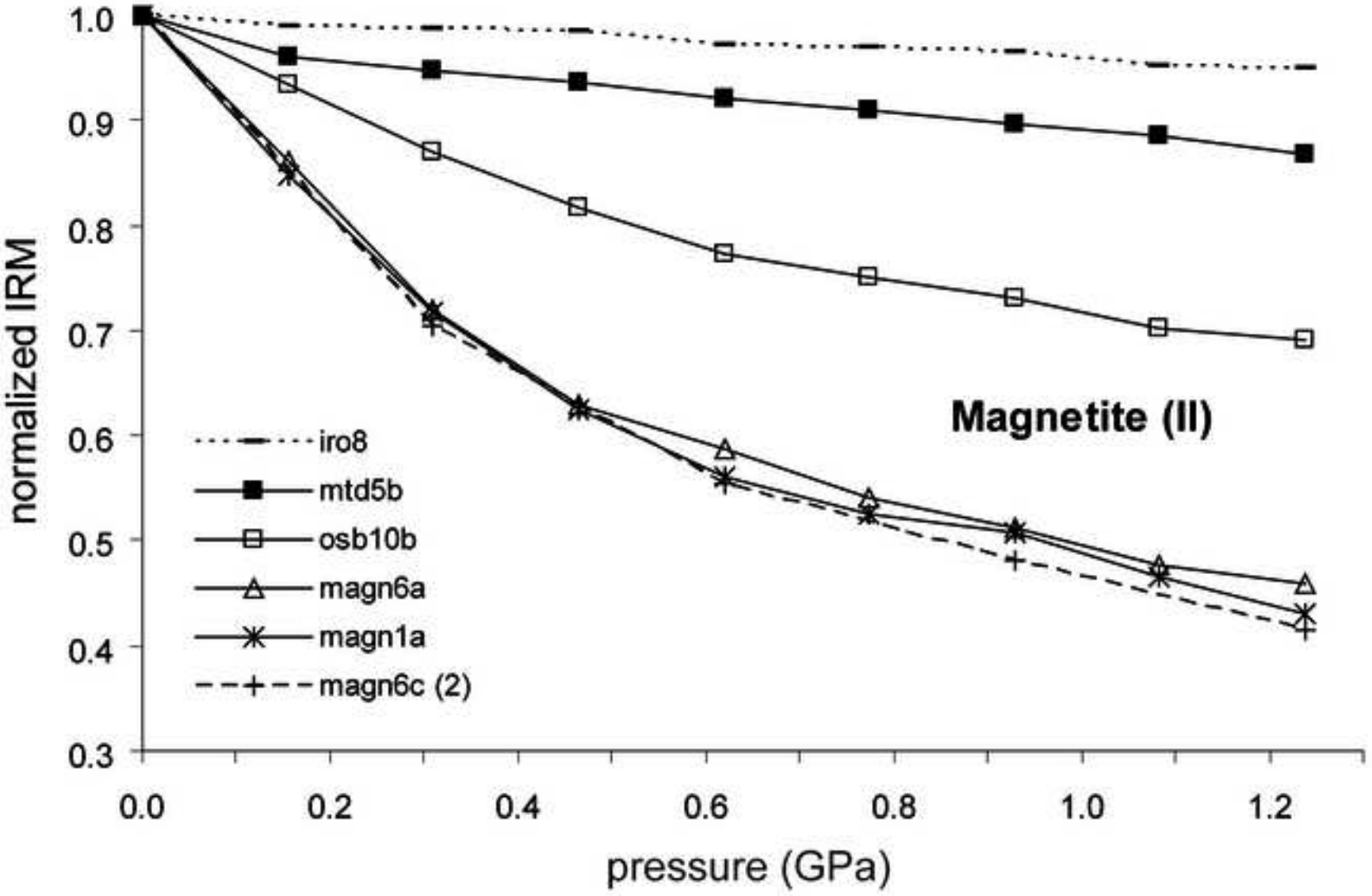
normalized IRM
1.0
0.9
0.8
0.7
0.6
0.5
0.4
0.3
0.0
0.2
0.4
0.6
0.8
1.0
1.2
pressure (GPa)
Magnetite (II)
iro8
mtd5b
osb10b
magn6a
magn1a
magn6c (2)

Figure(s)

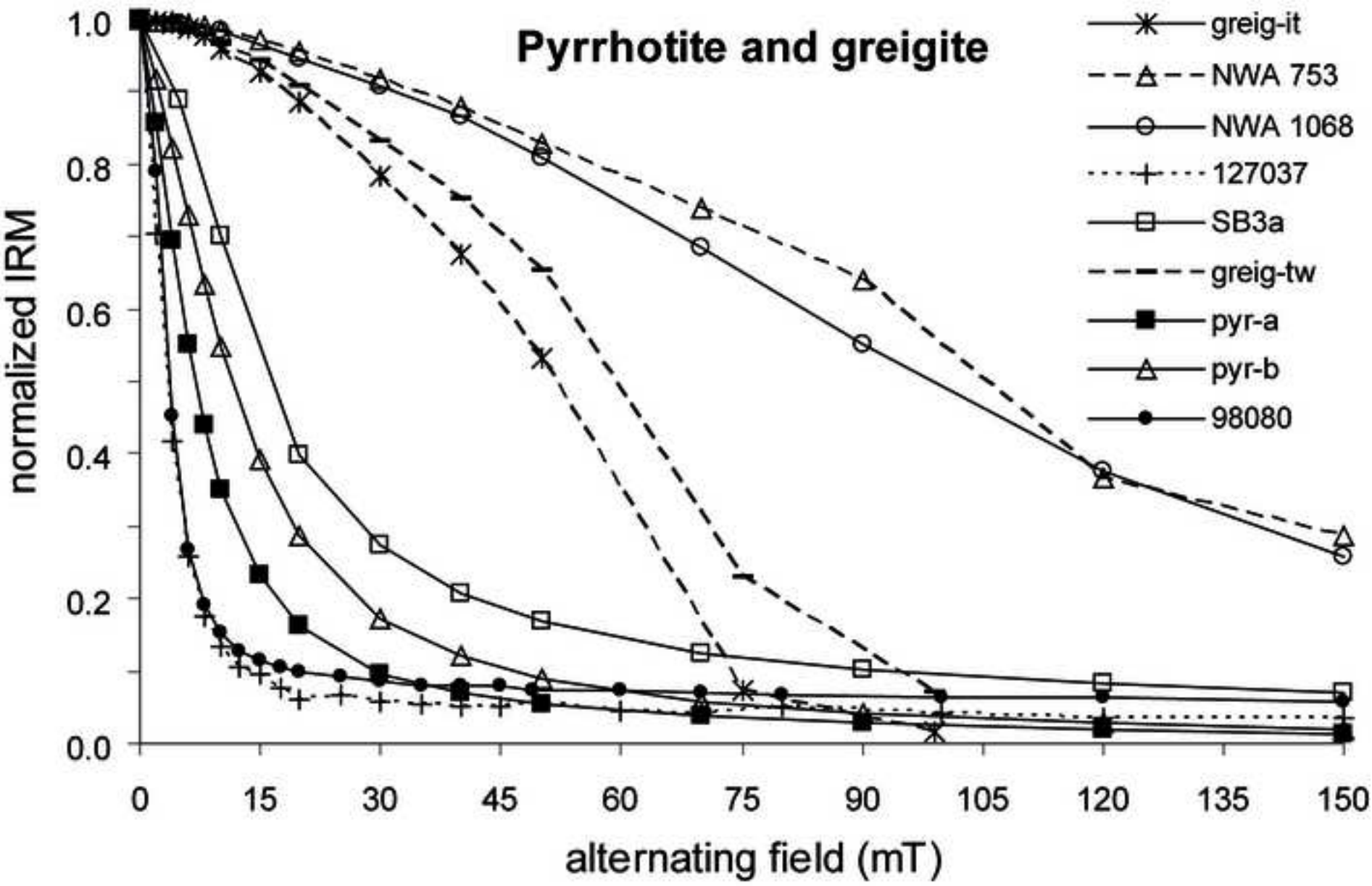
Pyrrhotite and greigite
normalized IRM
alternating field (mT)
1.0
0.8
0.6
0.4
0.2
0.0
0
15
30
45
60
75
90
105
120
135
150
greig-it
NWA 753
NWA 1068
127037
SB3a
greig-tw
pyr-a
pyr-b
98080

Figure(s)

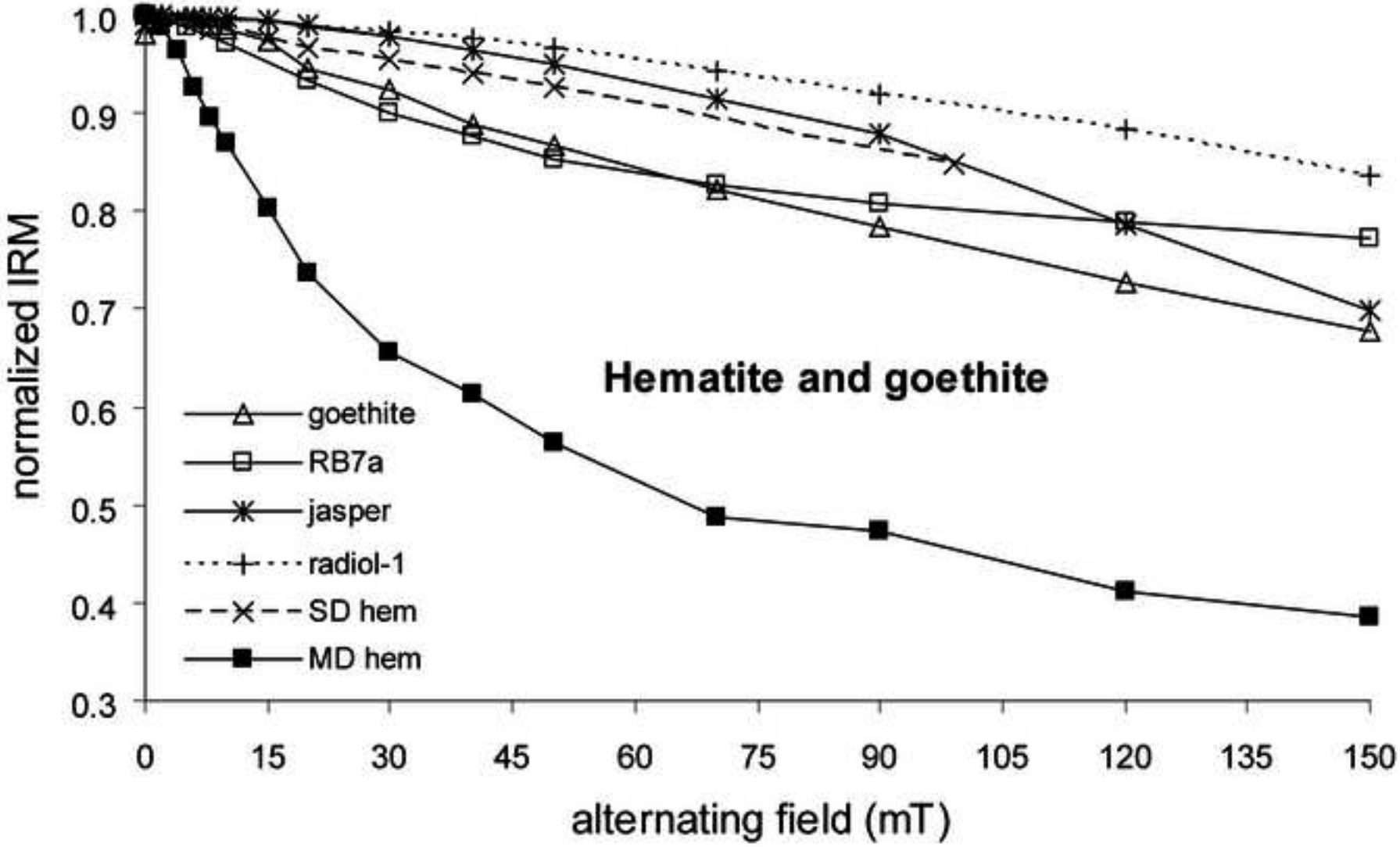
Hematite and goethite
normalized IRM
alternating field (mT)
1.0
0.9
0.8
0.7
0.6
0.5
0.4
0.3
0
15
30
45
60
75
90
105
120
135
150
goethite
RB7a
jasper
radiol-1
SD hem
MD hem

Figure(s)

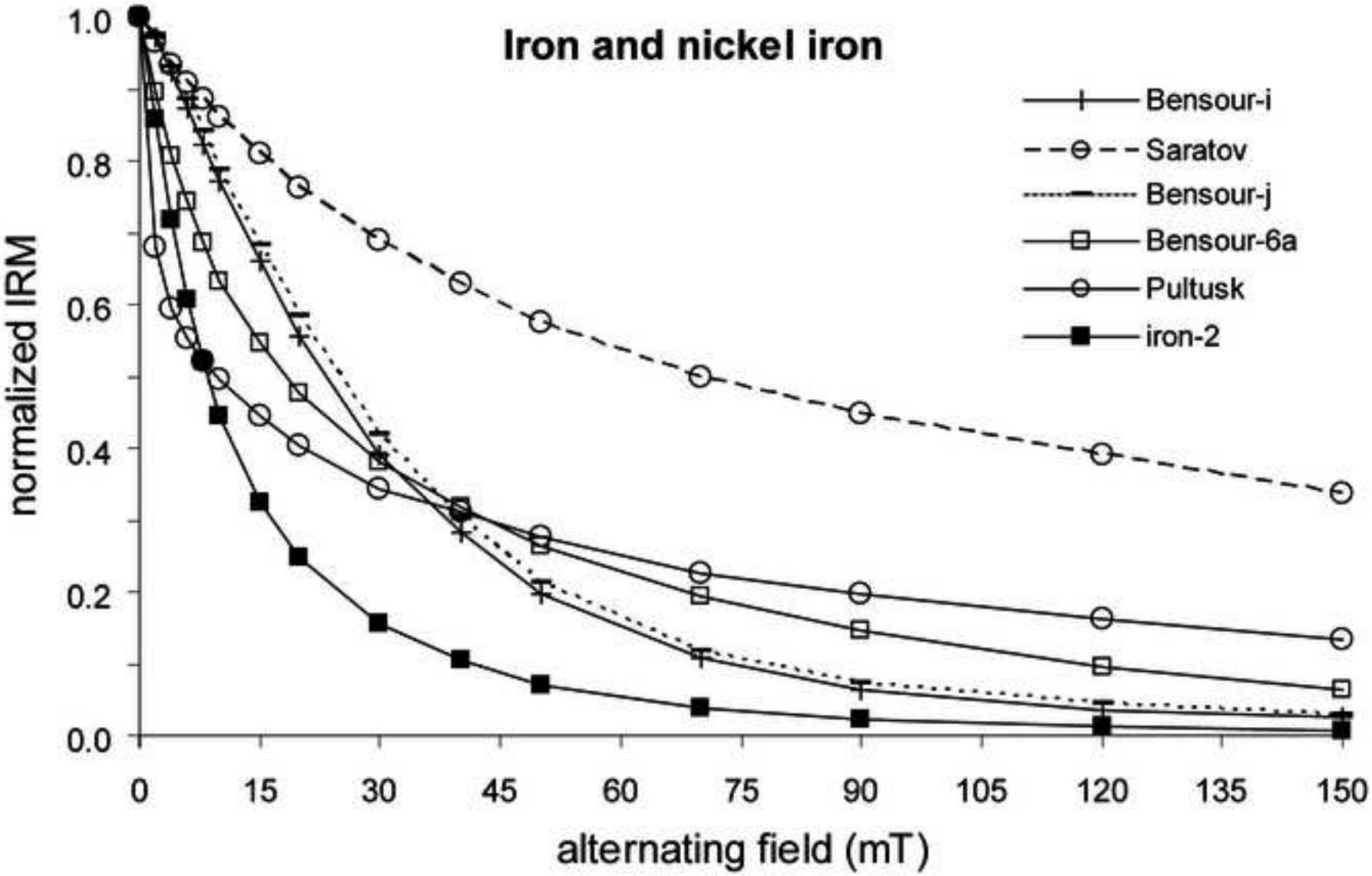
Iron and nickel iron
Bensour-i
Saratov
Bensour-j
Bensour-6a
Pultusk
iron-2
normalized IRM
1.0
0.8
0.6
0.4
0.2
0.0
0
15
30
45
60
75
90
105
120
135
150
alternating field (mT)

Figure(s)

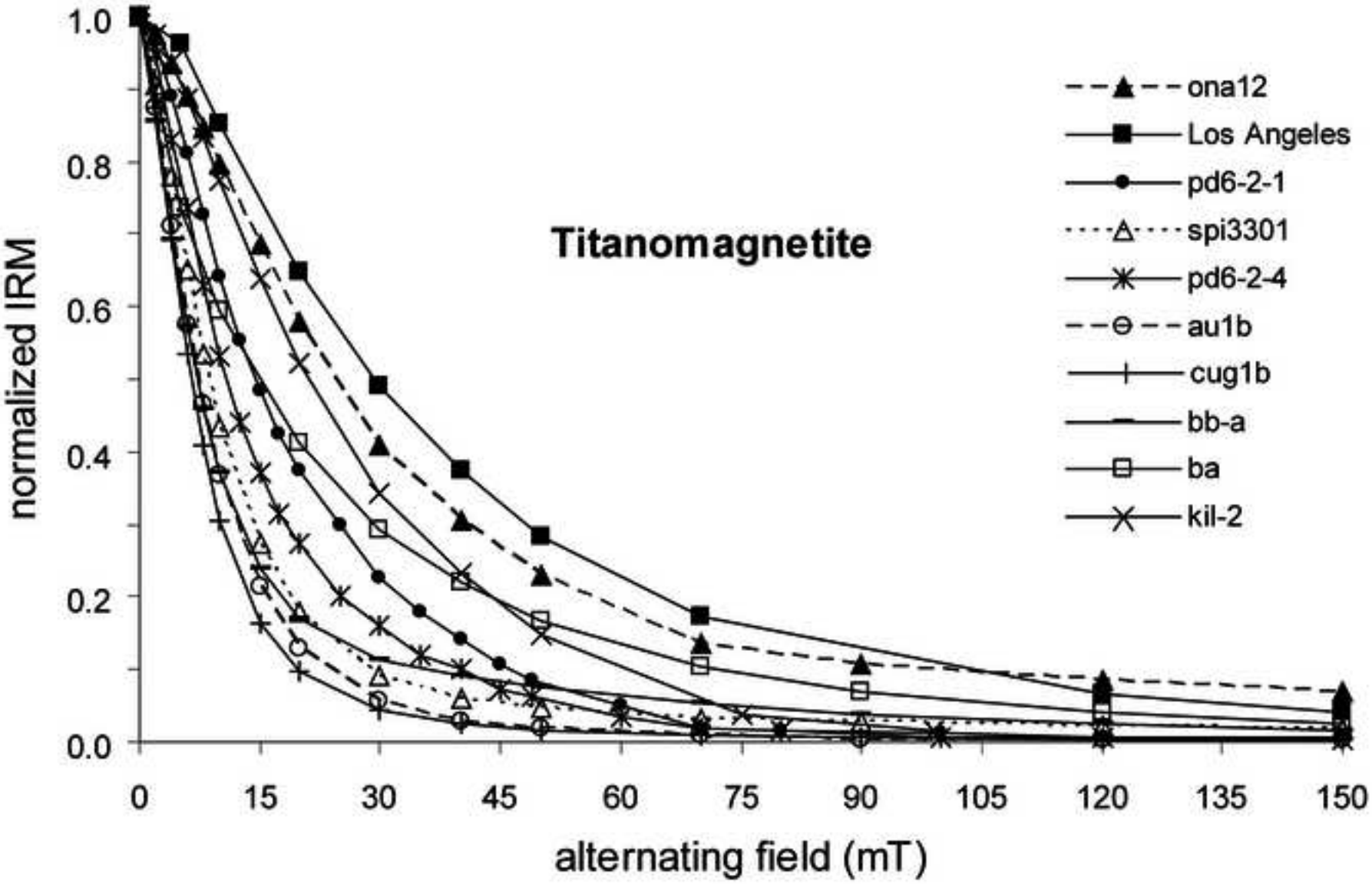
Titanomagnetite
normalized IRM
alternating field (mT)
1.0
0.8
0.6
0.4
0.2
0.0
0
15
30
45
60
75
90
105
120
135
150
ona12
Los Angeles
pd6-2-1
spi3301
pd6-2-4
au1b
cug1b
bb-a
ba
kil-2

Figure(s)

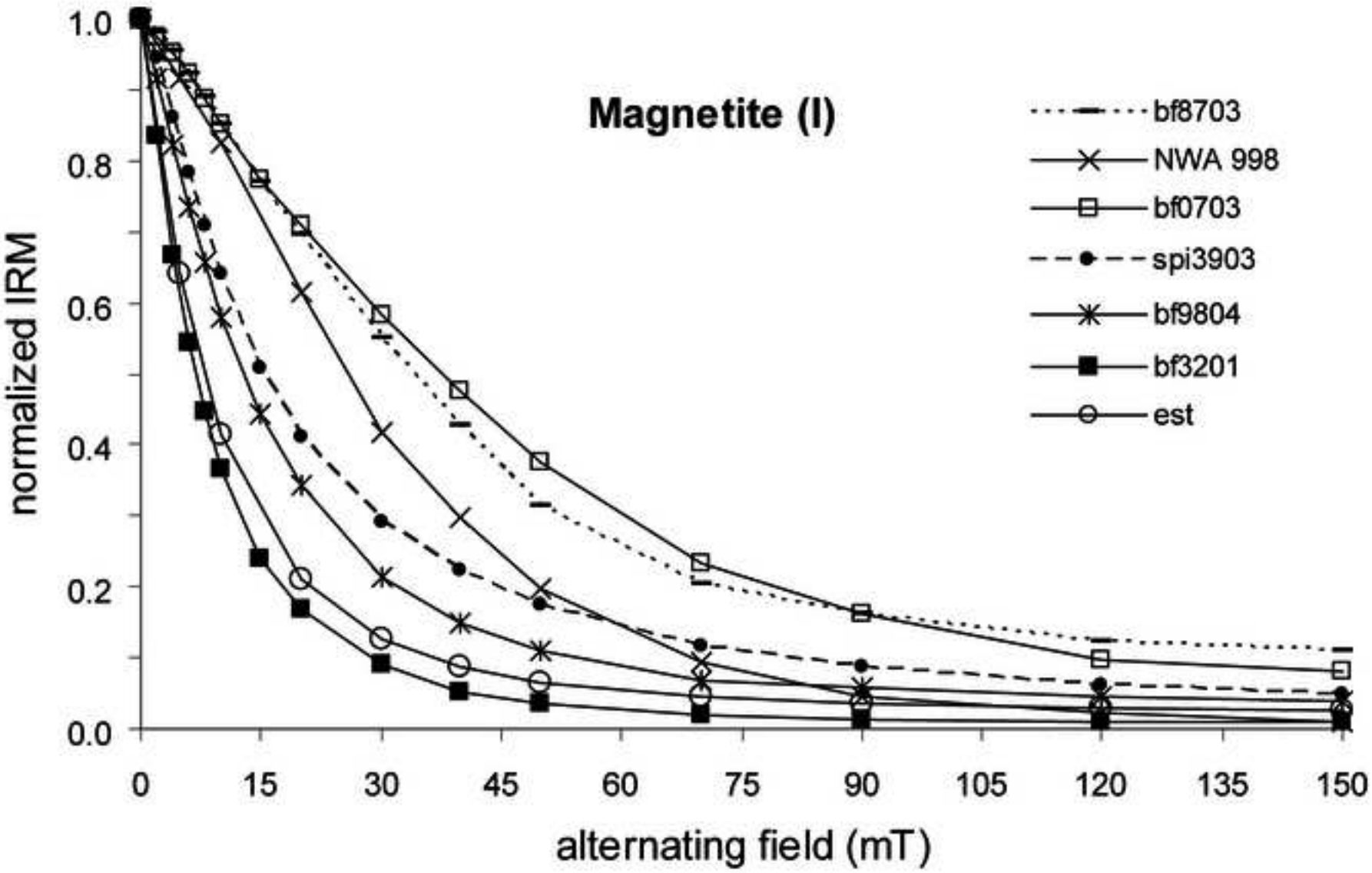
Magnetite (I)
normalized IRM
alternating field (mT)
1.0
0.8
0.6
0.4
0.2
0.0
0
15
30
45
60
75
90
105
120
135
150
bf8703
NWA 998
bf0703
spi3903
bf9804
bf3201
est

Figure(s)

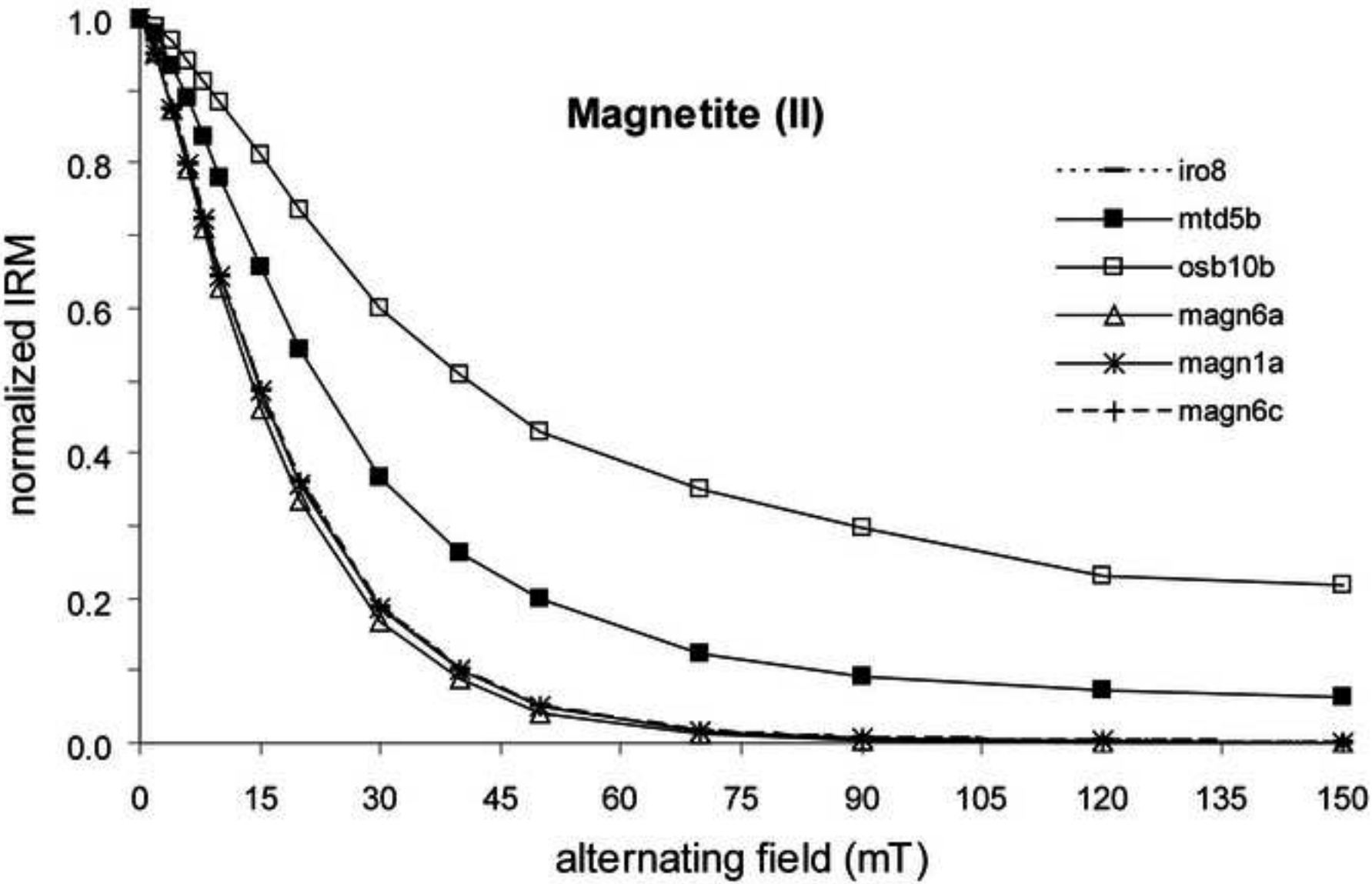
Magnetite (II)
normalized IRM
1.0
0.8
0.6
0.4
0.2
0.0
0
15
30
45
60
75
90
105
120
135
150
alternating field (mT)
iro8
mtd5b
osb10b
magn6a
magn1a
magn6c

Figure(s)

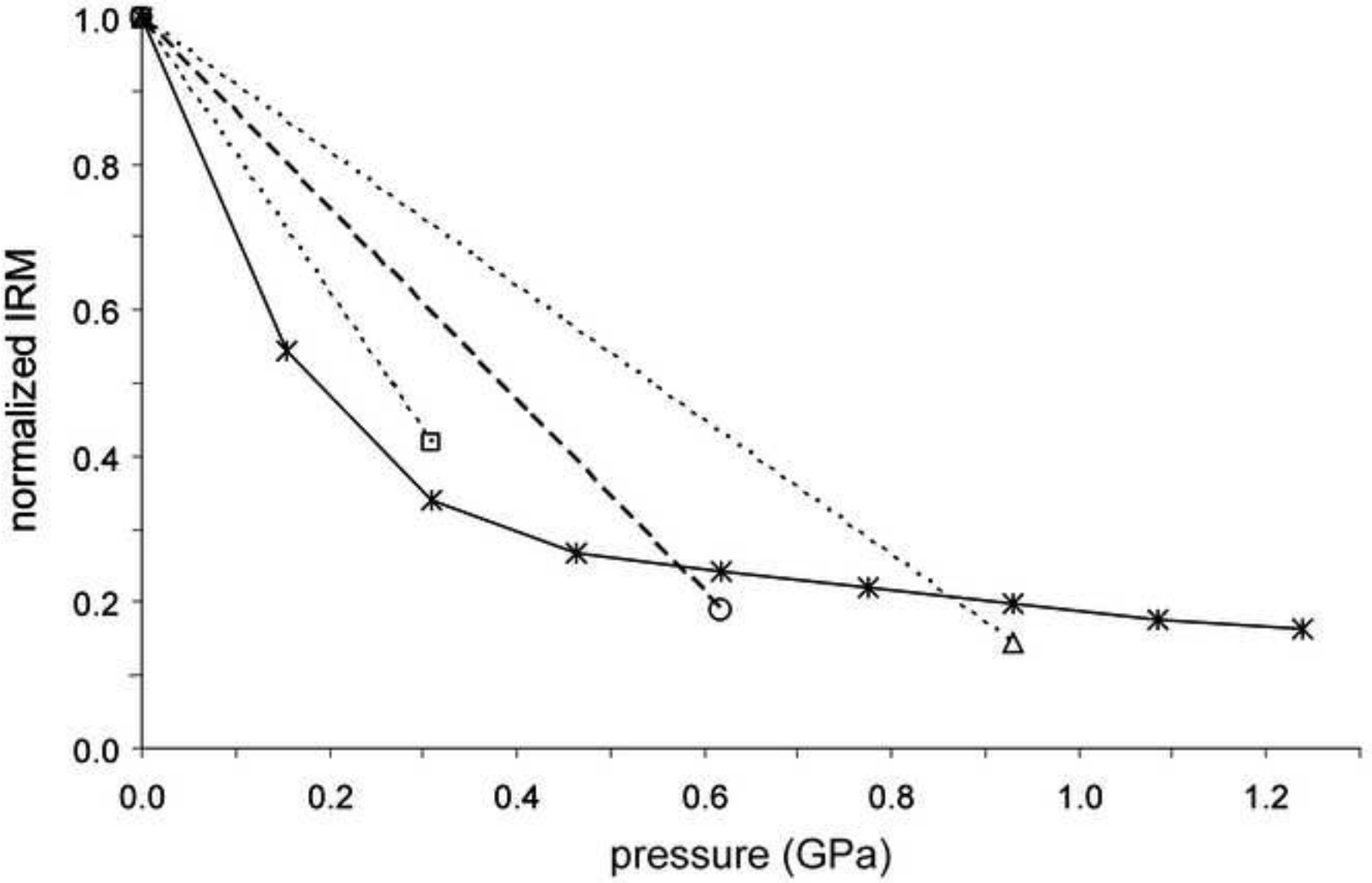
normalized IRM
1.0
0.8
0.6
0.4
0.2
0.0
0.0
0.2
0.4
0.6
0.8
1.0
1.2
pressure (GPa)

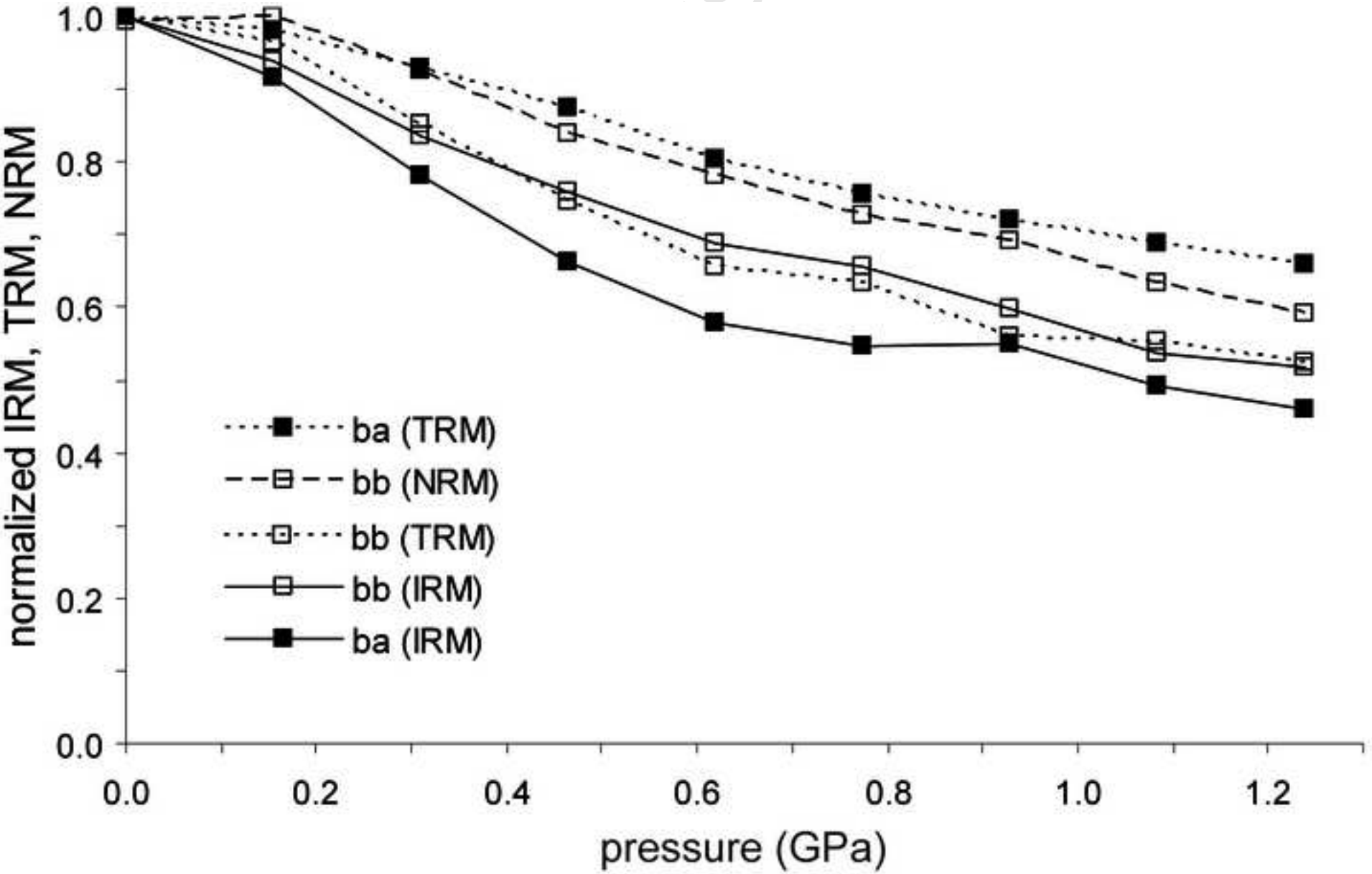
normalized IRM, TRM, NRM
1.0
0.8
0.6
0.4
0.2
0.0
0.0
0.2
0.4
0.6
0.8
1.0
1.2
pressure (GPa)
ba (TRM)
bb (NRM)
bb (TRM)
bb (IRM)
ba (IRM)

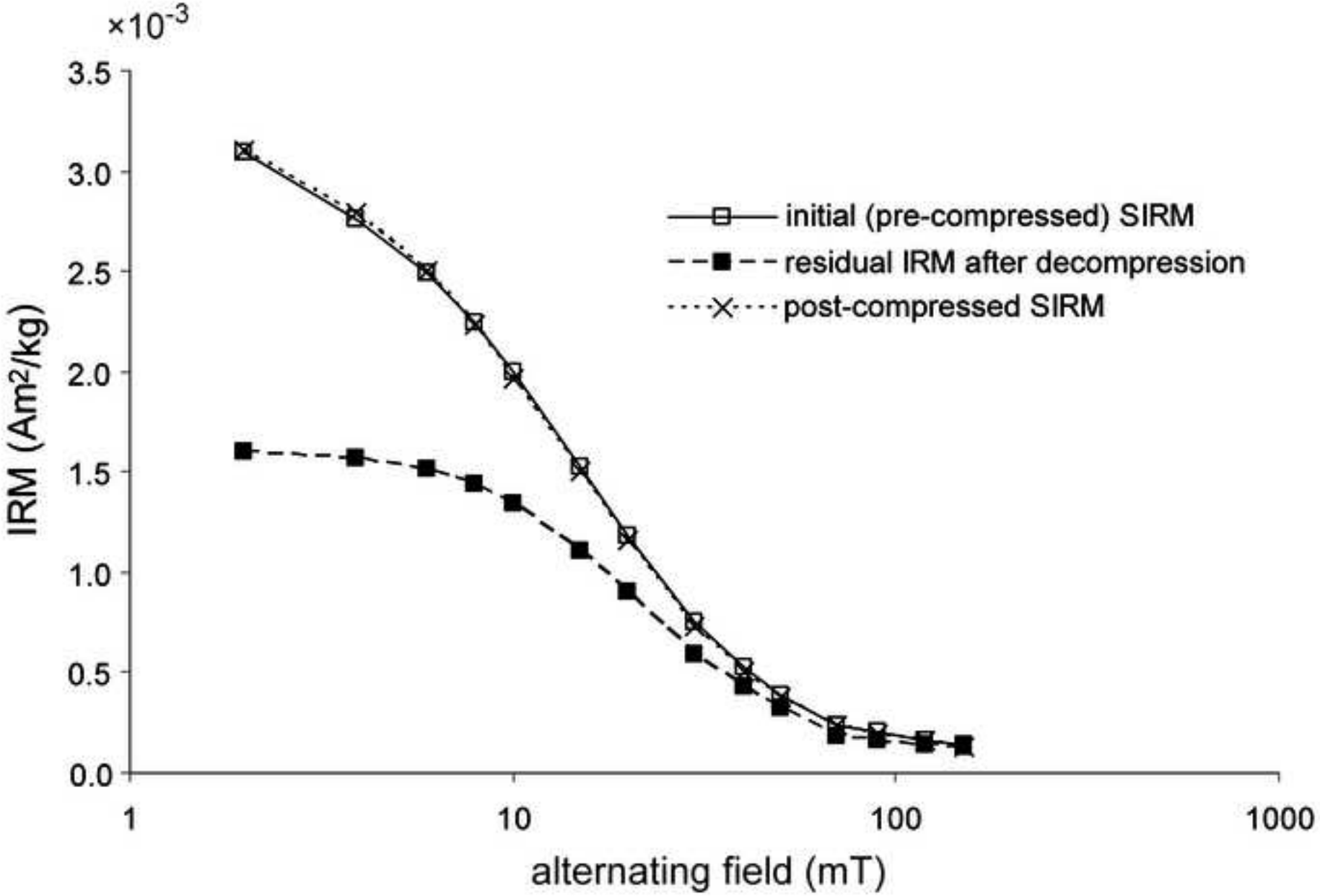
×10-3
3.5
3.0
2.5
2.0
1.5
1.0
0.5
0.0
IRM (Am²/kg)
initial (pre-compressed) SIRM
residual IRM after decompression
post-compressed SIRM
1
10
100
1000
alternating field (mT)

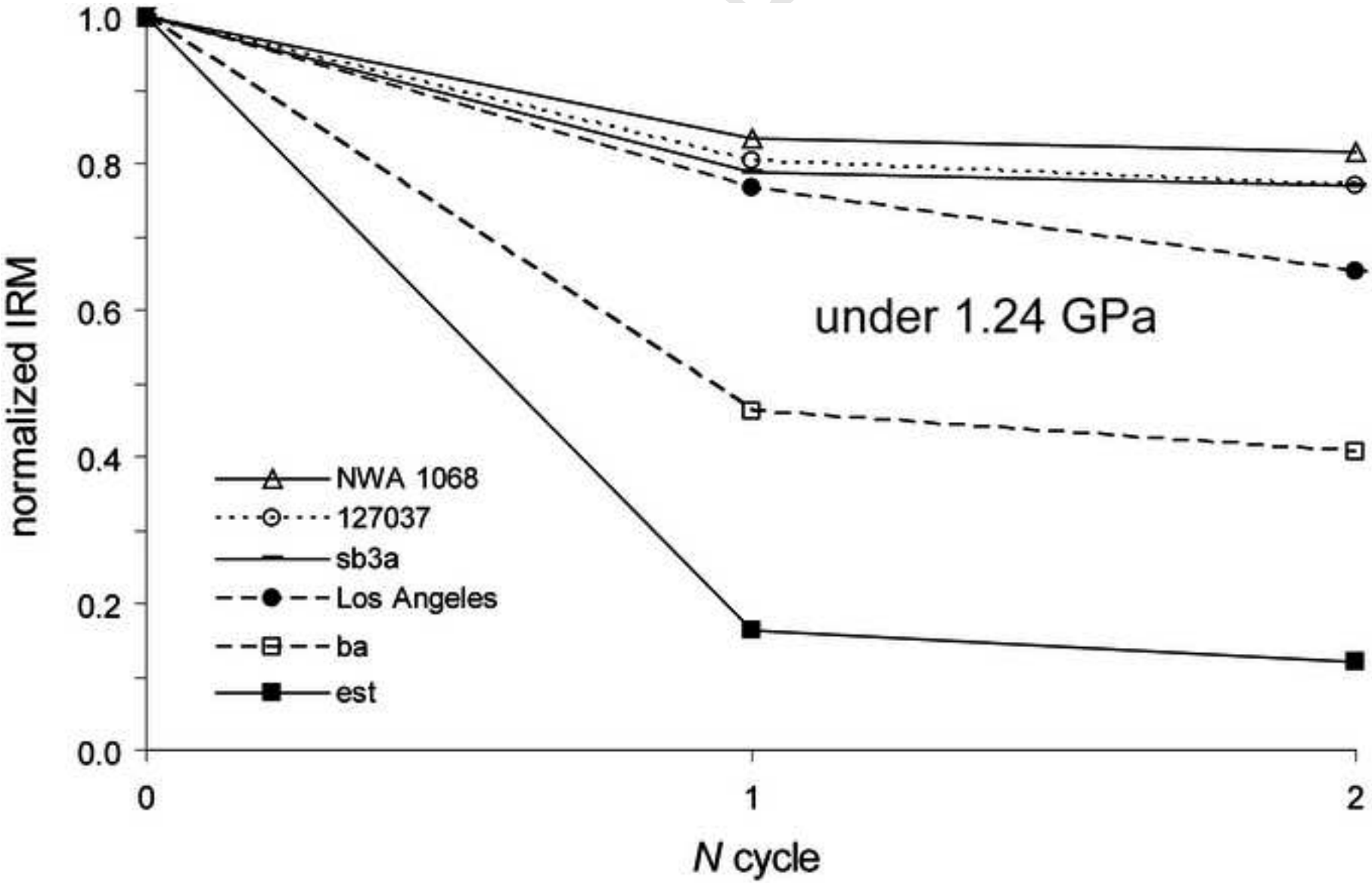
1.0
0.8
0.6
0.4
0.2
0.0
normalized IRM
0
1
2
N cycle
under 1.24 GPa
NWA 1068
127037
sb3a
Los Angeles
ba
est

Figure(s)

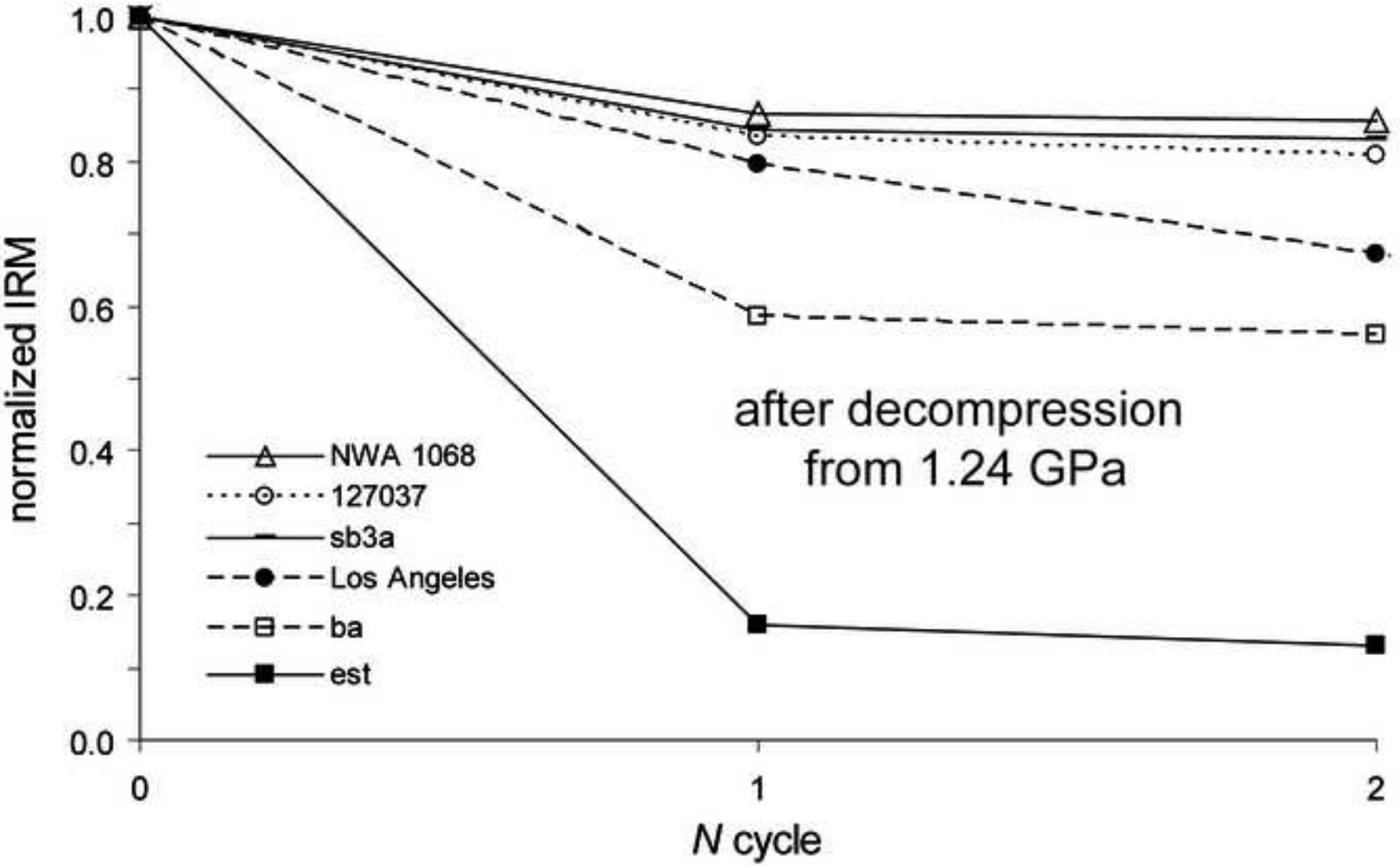
normalized IRM
1.0
0.8
0.6
0.4
0.2
0.0
0
1
2
N cycle
after decompression
from 1.24 GPa
NWA 1068
127037
sb3a
Los Angeles
ba
est

Figure(s)

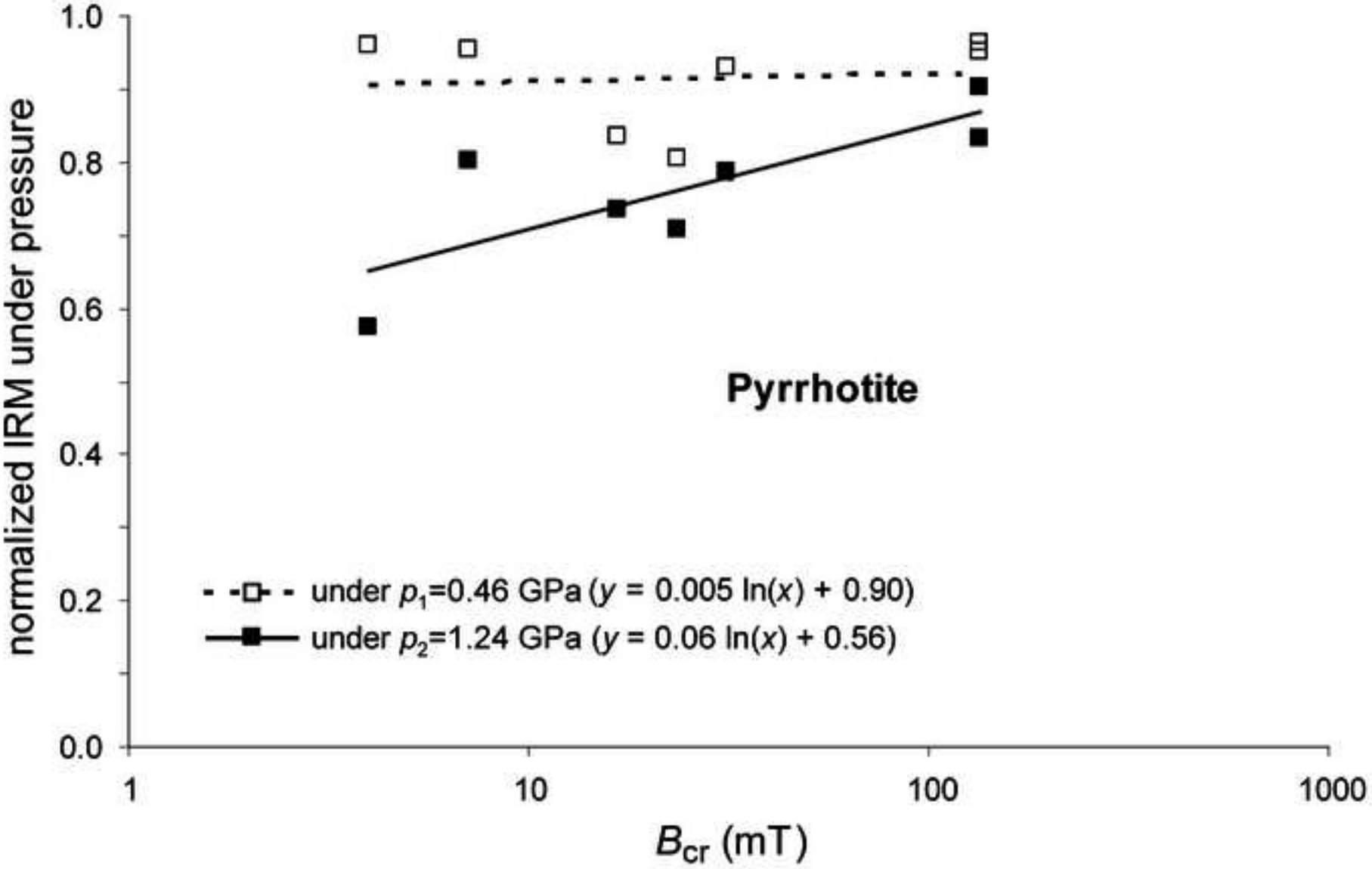
normalized IRM under pressure
1.0
0.8
0.6
0.4
0.2
0.0
1
10
100
1000
B_{cr} (mT)
Pyrrhotite
under p_1=0.46 GPa (y = 0.005 ln(x) + 0.90)
under p_2=1.24 GPa (y = 0.06 ln(x) + 0.56)

Figure(s)

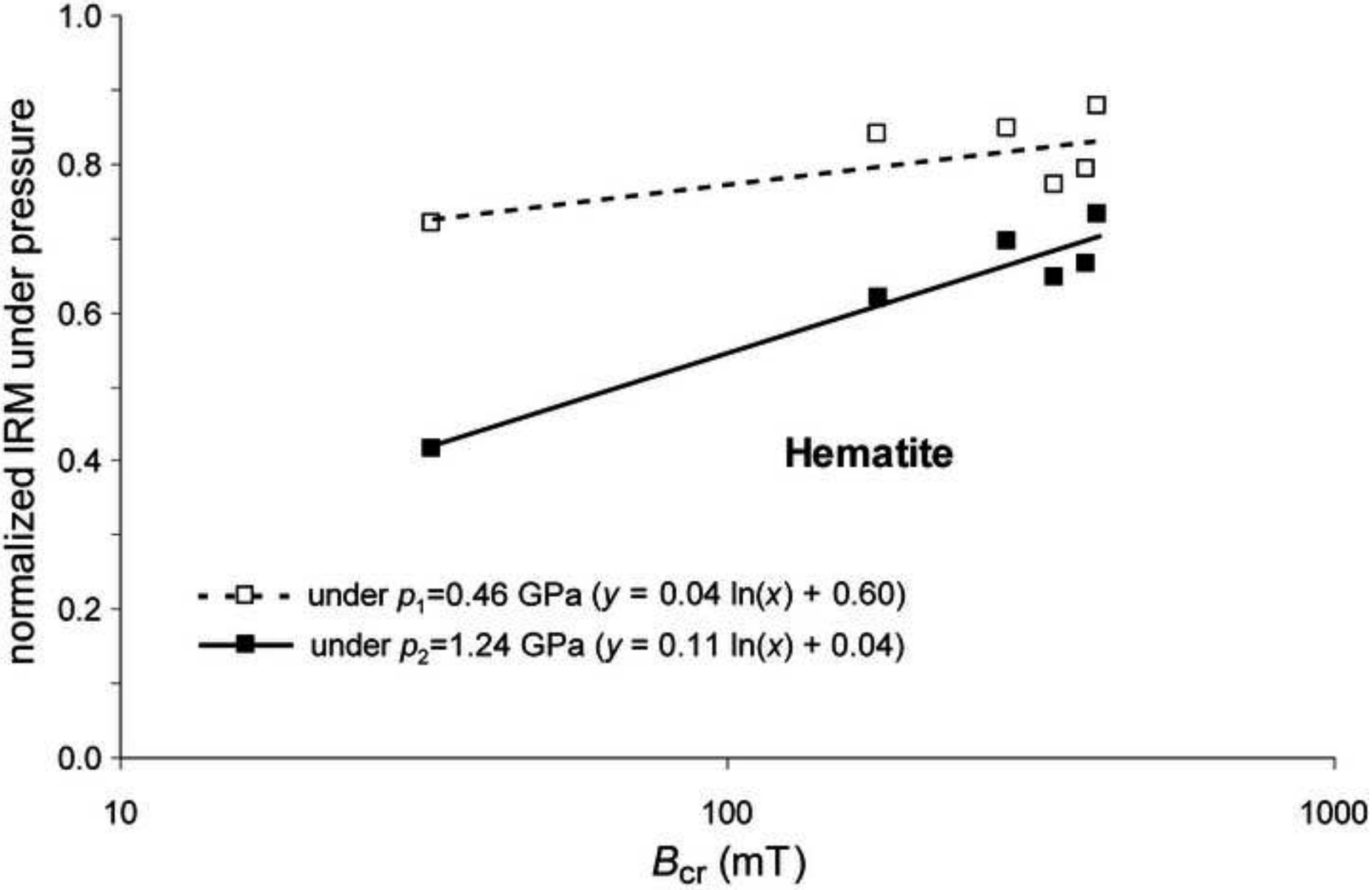
1.0
0.8
0.6
0.4
0.2
0.0
normalized IRM under pressure
Hematite
under p_1=0.46 GPa (y = 0.04 ln(x) + 0.60)
under p_2=1.24 GPa (y = 0.11 ln(x) + 0.04)
10
100
1000
B_{cr} (mT)

Figure(s)

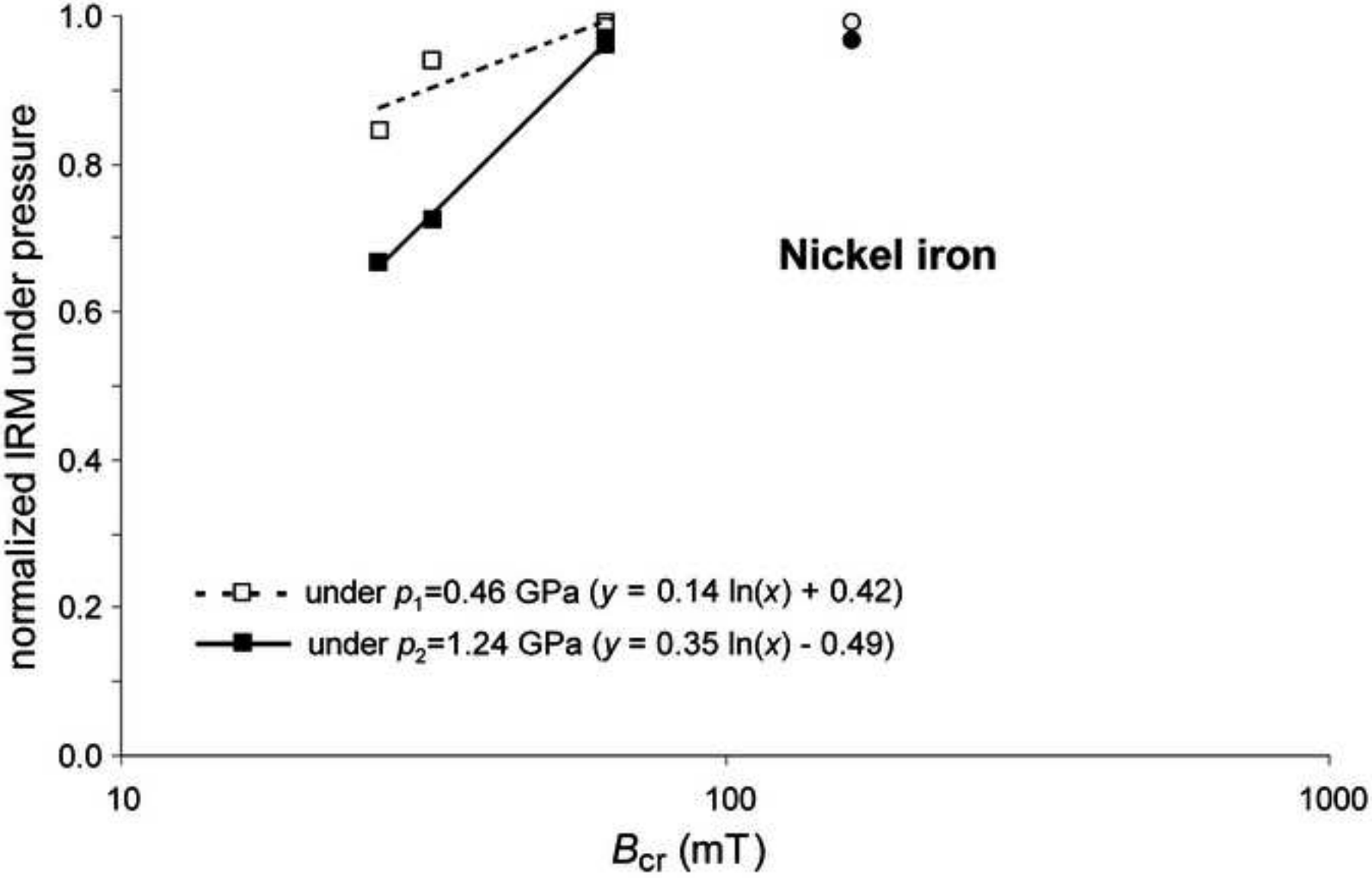
1.0
0.8
0.6
0.4
0.2
0.0
normalized IRM under pressure
Nickel iron
under p_1=0.46 GPa (y = 0.14 ln(x) + 0.42)
under p_2=1.24 GPa (y = 0.35 ln(x) - 0.49)
10
100
1000
B_{cr} (mT)

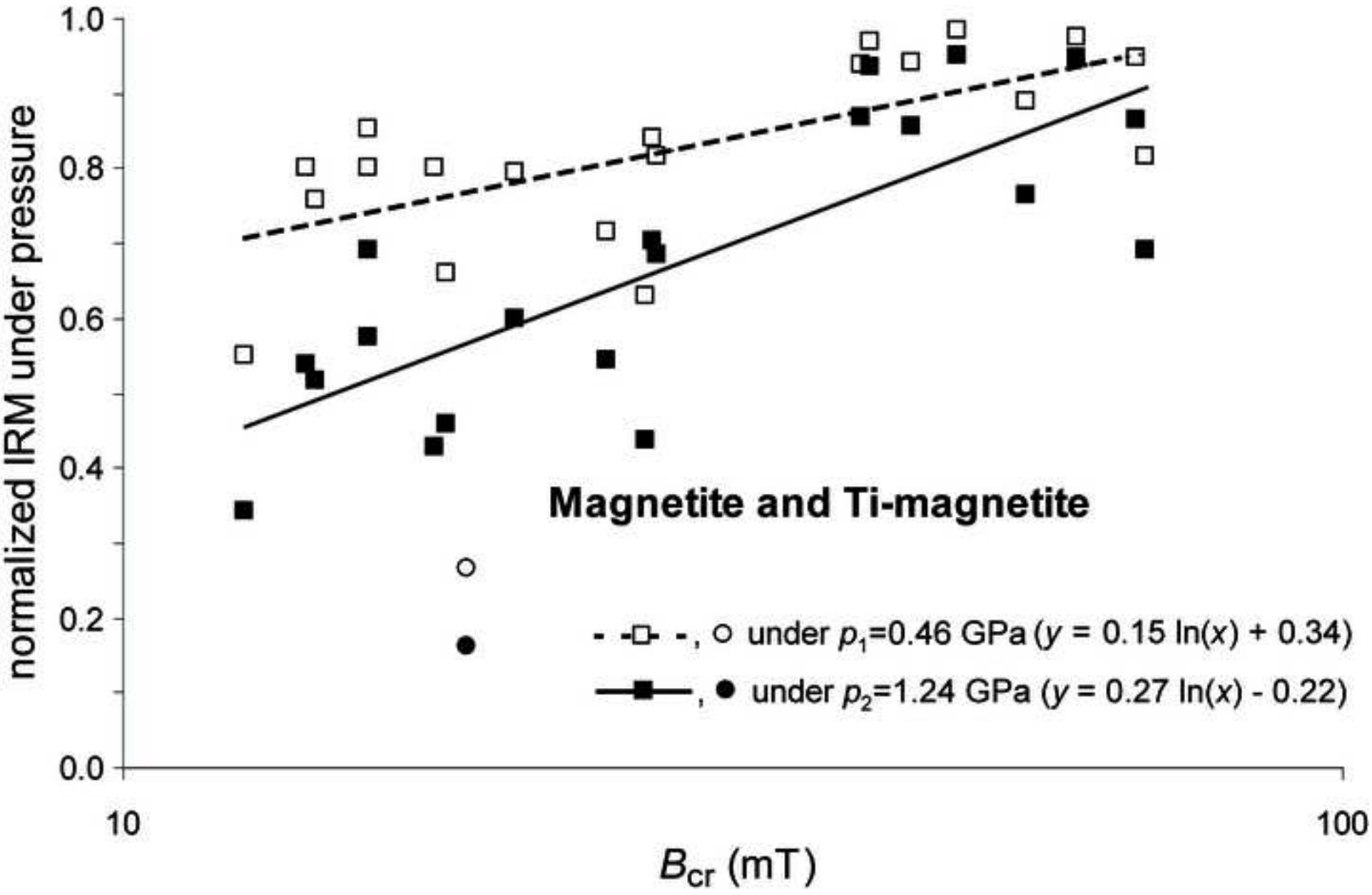
1.0
0.8
0.6
0.4
0.2
0.0
normalized IRM under pressure
Magnetite and Ti-magnetite
under p_1=0.46 GPa (y = 0.15 ln(x) + 0.34)
under p_2=1.24 GPa (y = 0.27 ln(x) - 0.22)
10
100
B_{cr} (mT)

Figure(s)

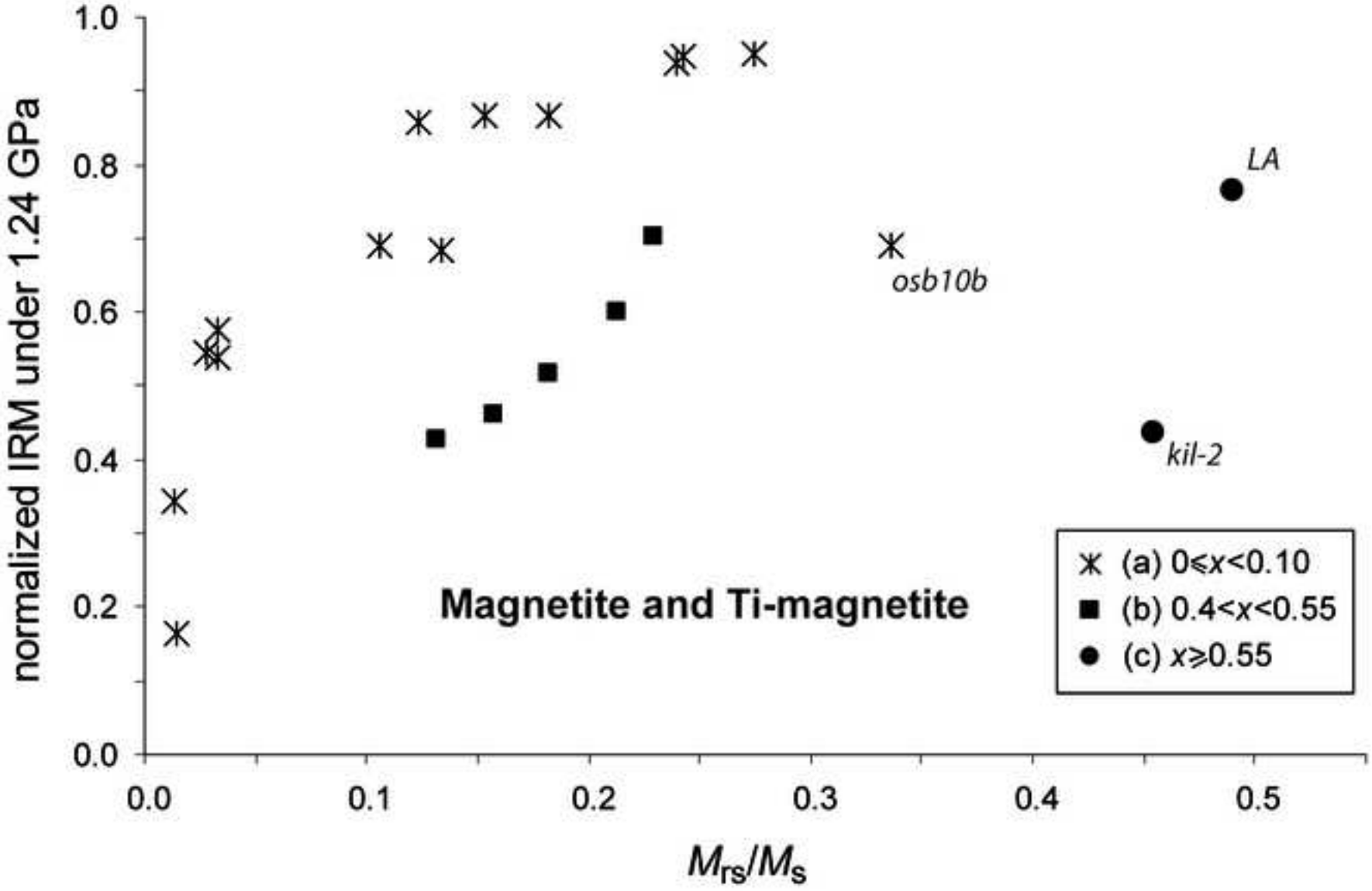
normalized IRM under 1.24 GPa
1.0
0.8
0.6
0.4
0.2
0.0
0.0
0.1
0.2
0.3
0.4
0.5
M_{rs}/M_s
LA
osb10b
kil-2
Magnetite and Ti-magnetite
(a) 0≤x<0.10
(b) 0.4<x<0.55
(c) x≥0.55

Figure(s)

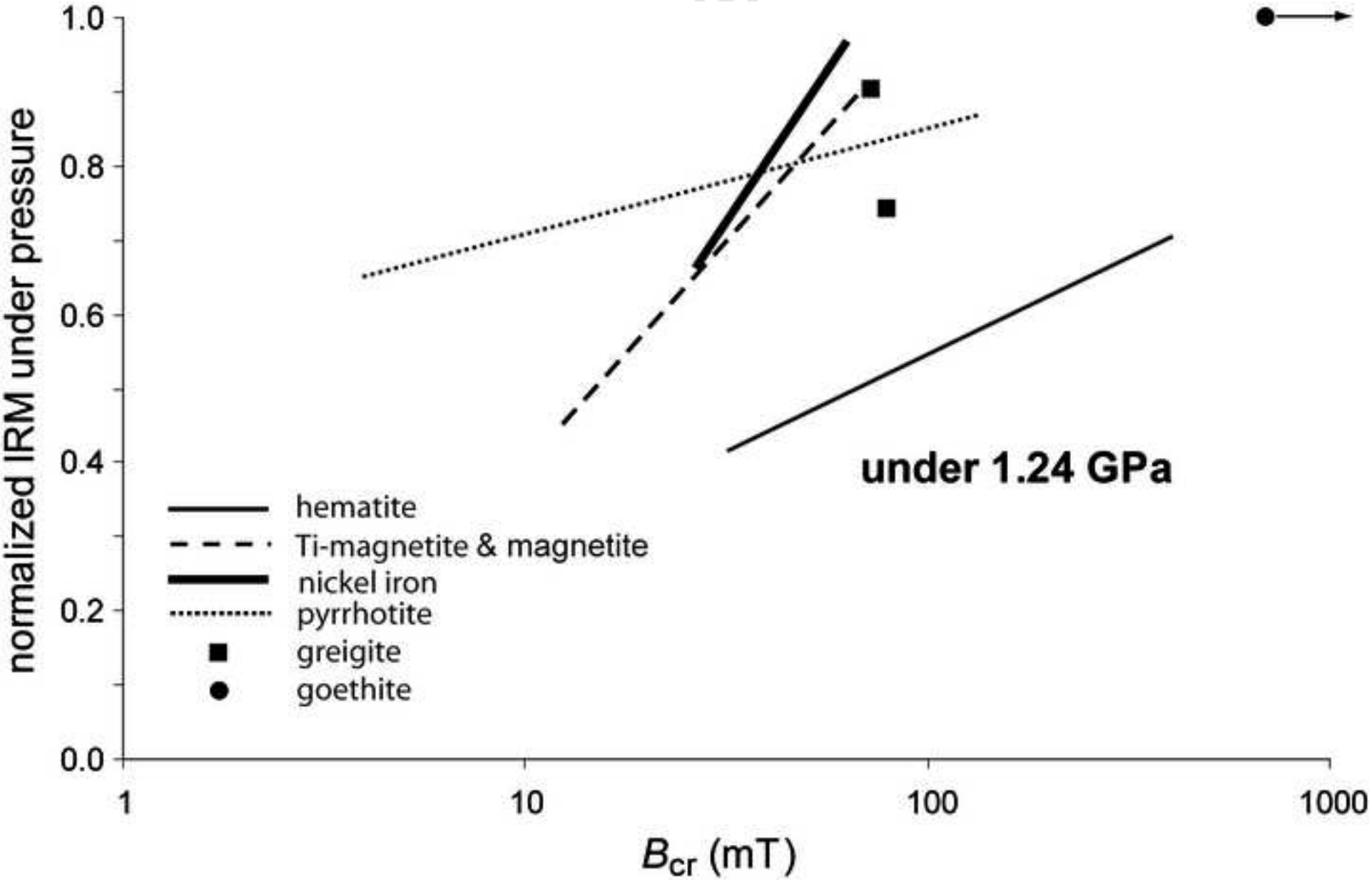
normalized IRM under pressure
1.0
0.8
0.6
0.4
0.2
0.0
1
10
100
1000
B_{cr} (mT)
under 1.24 GPa
hematite
Ti-magnetite & magnetite
nickel iron
pyrrhotite
greigite
goethite

TABLES

Table 1

Main magnetic properties of investigated samples.

Sample	Main magnetic carrier and ref.	m	T_C	χ_0	MDF_i	B_{cr}	B_{cr}/B_c	M_s	M_{rs}/M_s
METEORITES									
Martian meteorites									
Los Angeles	Ti-magn [11, 13]	94.3	150	10.3	31	55	1.41	1232	0.49
NWA 1068	pyrrhotite [13, 11]	240.2	*325*	1.3	100	134	1.54	212	0.47
NWA 998	magnetite [13, 11]	20.4	*575*	4.3	25	41	1.73	713	0.24
Ordinary chondrites									
Bensour-6a	taenite [0, 1]	162.0	*450*	154.0	18	33	35.8	3187	0.003
Bensour-i	tetrataenite [0, 1]	23.7	580	-	24	64	1.62	1963	0.16
Bensour-j	tetrataenite [0, 1]	102.4	580	46.8	25	64	1.62	1963	0.16
Pultusk	kamacite [0]	64.2	*760*	600.0	10	27	26.0	303	0.007
Saratov	tetrataenite [0]	54.1	*580*	633.0	70	162	35.8	16540	0.03
Rumuruti chondrites									
NWA 753	pyrrhotite [0, 15]	211.9	*325*	8.7	108	134	1.68	93	0.41
TERRESTRIAL ROCKS AND MINERALS									
Basalts									
ba	Ti-magn [9]	59.5	50	16.1	15	18	3.54	622	0.16
ba (TRM)	Ti-magn [9]	405.0	50	16.1	15	18	3.54	622	0.16
bb-a	Ti-magn [0, 6]	327.8	60/150	16.1	8	14	2.29	866	0.18
bb-a (TRM)	Ti-magn [0, 6]	327.3	60/150	16.1	8	14	2.29	866	0.18
bb-b (NRM)	Ti-magn [0, 6]	392.3	60/150	16.1	9	14	2.29	866	0.18
be-3a	Ti-magn [3, 10]	267.7	245	10.8	13	18	2.57	1700	0.13
pd6-2-1	Ti-magn [0, 8]	30.8	280	109.0	15	27	1.86	1827	0.23
pd6-2-4	Ti-magn [0, 8]	51.2	280	131.0	11	21	1.79	1833	0.21
Andesites									
au1b	Ti-magn [0, 5]	226.2	530	121.4	8	16	4.24	1828	0.03
cug1b	Ti-magn [0, 5]	175.5	550	88.7	7	14	4.65	1048	0.03
osb10b	magnetite [0, 5]	125.3	575	9.74	40	69	2.10	139	0.34
Ignimbrites									
spi3301	Ti-magn [0, 5]	302.8	560	73.0	9	16	2.81	545	0.11
ona12	Ti-magn [0, 5]	109.4	560	45.4	24	44	2.86	787	0.12
spi3903	magnetite [0, 5]	233.0	575	54.1	16	27	2.79	621	0.13
mtd5b	magnetite [0, 5]	162.3	575	93.7	22	40	2.37	1356	0.18
iro8	magnetite [0, 5]	161.0	575	13.6	31	48	2.03	151	0.27
Rhyolites									
rb7a	hematite [16]	238.0	650	0.03	>150	406	3.56	5	0.48
Radiolarites									
radiol-1	hematite [0]	333.5	675	1.4	>150	390	1.21	67	0.68

Sample	Main magnetic carrier and ref.	m	T_C	χ_0	MDF_i	B_{cr}	B_{cr}/B_c	M_s	M_{rs}/M_s
radiol-2	hematite [0]	232.1	675	1.6	>150	347	1.30	74	0.69
Granites									
bf0703	magnetite [0, 2]	304.6	575	11.6	39	68	2.98	165	0.15
bf3201	magnetite [0, 2]	425.5	575	41.3	7	13	7.54	448	0.01
bf9804	magnetite [0, 2]	453.3	575	8.8	13	25	6.01	112	0.03
bf8703	magnetite [0, 2]	228.0	575	3.8	34	61	2.08	76	0.24
Microdiorite									
est	magnetite [4]	320.0	575	13.5	8	19	10.3	128	0.01
Schist									
sb3a	pyrrhotite [4]	243.3	280/320	0.3	17	31	1.29	91	0.50
Jasper									
jas	hematite [0]	210.0	675	4.1	>150	289	1.38	154	0.70
Obsidian									
kil-2	Ti-magn [0]	219.4	142	4.4	21	27	1.34	822	0.45
Minerals (monocrystals)									
98080	pyrrhotite [0, 7]	429	325	11.8	4	4	0.88	1444	0.46
127037	pyrrhotite [0, 7]	24.5	325	6.2	3	7	1.51	5696	0.15
goethite	goethite [0, 14]	320.1	~120	0.3	>150	>9000	-	-	-
Sediments									
greig-tw1	greigite [17]	5.0	*330*	970	59	80	1.38	19470	0.52
greig-it1	greigite [18]	4.1	*330*	1408	52	73	1.45	29073	0.45
SYNTHETIC SAMPLES of dispersed powders in epoxy resin									
pyr-a (20.5; 5.2)	pyrrhotite [0, 12]	33.5	*325*	175	7	17	1.73	-	0.21
pyr-b (13.1; 3.4)	pyrrhotite [0, 12]	32.8	*325*	69.2	11	23	1.51	-	0.32
magn1a (0.3; 0.1)	magnetite [0]	170.0	*575*	15.1	15	32	3.22	-	0.08
magn6a (17.3; 4)	magnetite [0]	73.6	*575*	-	14	28	3.02	-	0.09
magn6c (0.8; 0.2)	magnetite [0]	89.4	*575*	-	15	29	3.03	-	0.09
magn6d (0.5; 0.1)	magnetite [0]	79.4	*575*	-	15	30	3.10	-	0.09
iron-2 (2.5; 0.4)	iron [0]	229.5	753	281	8	22	13.8	-	0.004
MD hem (2.1; 0.5)	hematite [0]	116.1	*675*	0.95	67	33	1.11	-	0.57
SD hem	hematite [0]	155.6	*675*	-	>100	177	1.43	-	0.73

m is mass (in mg). T_C is Curie temperature (in °C); theoretical value when italized. χ_0 is low field magnetic susceptibility (in $10^{-6}m^3/kg$). MDF_i is median destructive field of IRM (in mT): 9T IRM for hematite-bearing and goethite samples and 3T IRM for all other samples. B_c and B_{cr} are magnetic coercivity and coercivity of remanence, respectively (in mT). M_s and M_{rs} are saturation and saturation remanent magnetization (in 10^{-3} Am^2/kg). "Ti-magn" is titanomagnetite. For synthetic samples numbers between brackets (1st column) correspond to estimated mass and volume concentrations of powders in the sample respectively (in %) and mass values correspond to the mass of the whole samples of dispersed powder with epoxy resin matrix. In the second column the information between brackets

corresponds to reference(s) where samples are described and/ or their magnetic properties measured. [(0)] this study; [(1-6)] Gattacceca et al., 2003, 2004, 2006, 2007a, 2007b and 2008, respectively; [(7-8)] Louzada et al., 2007, 2008; [(9-15)] Rochette et al., 1993, 1998, 2001, 2003, 2005a, 2005b, 2008, respectively; [(16)] Vlag. et al., 1997; [(17, 18)] {Horng et al., 1998; Jiang et al., 2001} and {Florindo et al., 1995; Van Dongen et al., 2007}, respectively.

Table 2.

Synthesis of results on pressure demagnetization experiments.

Sample	$SIRM_1$	IRM_{p2}	Δ	IRM_{PR}	δ	$SIRM_2$	MDS	α	ε_1
pressure cell [(1)]	0.0343	0.0433	-	-	-	-	-	-	-
METEORITES									
Los Angeles	11.9	9.11	23	3.08	3.1	9.20	*2.5*	1.3	21(67)
NWA 1068	25.3	21.1	17	19.8	3.2	24.6	*3.7*	0.8	36(20)
NWA 998	7.97	7.47	6	6.25	-0.4	7.36	*9.5*	1.1	69(15)
Bensour-6a	1.36	1.10	19	1.01	-3.7	1.57	*3.1*	0.8	80(36)
Bensour-i	6.81	6.60	3	6.49	2.1	6.28	*22.4*	1.3	-
Bensour-j	32.0	30.7	4	30.6	-0.9	32.0	*13.3*	1.0	46(4)
Pultusk	15.3	10.2	33	9.89	0	16.0	*1.8*	1.3	98(38)
Saratov	20.3	19.6	3	18.5	0.5	-	*18.9*	0.8	20(16)
NWA 753	7.80	7.05	10	6.94	1.3	7.65	6.5	1.0	44(9)
TERRESTRIAL ROCKS AND MINERALS									
ba	6.78	3.12	54	3.56	12.5	6.13	1.07	1.7	29(42)
ba [(2)]	5.52	3.64	34	-	10.9	-	*1.7*	1.0	-
bb-a	48.3	24.9	48	25.7	1.9	52.5	*1.26*	1.4	95(51)
bb-a [(2)]	2.12	1.11	48	1.63	5.1	52.5	*1.26*	1.5	4(97)
bb-b [(3)]	1.62	0.96	40	0.91	9.1	2.12	1.5	1.0	72(57)
be-3a	74.9	32.1	57	36.9	6.8	71.7	1.08	-	91(48)
pd6-2-1	12.1	8.51	30	8.91	3.9	12.1	*2.6*	1.5	99(26)
pd6-2-4	18.5	11.1	40	10.6	2.2	19.1	*1.6*	1.4	97(45)
au1b	13.1	7.55	42	7.62	0.3	12.7	*1.4*	1.3	-
cug1b	5.62	3.04	46	2.62	-6.9	5.92	*1.29*	1.2	88(56)
osb10b	5.64	3.89	31	4.22	5.7	5.91	2.6	1.6	59(29)
spi 3301	19.1	13.2	31	10.4	-7.3	16.5	*1.9*	1.3	81(37)
ona12	10.4	8.91	14	8.72	0.2	10.4	*4.2*	1.1	89(16)
spi3903	18.1	12.4	31	12.1	1.7	18.3	*2.7*	1.6	75(34)
mtd5b	38.0	33.0	13	37.5	-3.9	37.2	*5.1*	1.4	75(19)
iro8	6.37	6.05	5	5.73	-0.2	6.20	12.4	0.8	88(8)
rb7a	0.55	0.40	27	0.44	8.9	0.60	*2.1*	1.2	14(27)
radiol-1	17.9	11.9	34	11.7	0.0	18.7	*2.3*	1.7	3(38)
radiol-2	13.2	8.53	35	9.45	8.1	13.5	*2.0*	1.7	6(30)
bf0703	9.47	8.22	13	7.80	-2.5	8.47	*4.7*	1.1	-
bf3201	2.76	0.95	66	0.75	-4.6	2.72	0.54	1.8	65(73)
bf9804	1.41	0.77	46	0.73	-3.9	1.54	*1.5*	1.7	66(53)
bf8703	4.14	3.92	5	3.79	-1.7	4.13	*11.9*	1.2	61(8)
est	8.09	1.32	84	0.98	-0.5	8.17	0.19	2.4	43(88)
sb3a	15.5	12.2	22	11.8	5.8	20.3	3.7	0.9	25(42)

Sample	$SIRM_1$	IRM_{p2}	Δ	IRM_{PR}	δ	$SIRM_2$	MDS	α	ε_1
jas	24.3	16.9	30	18.2	6.6	23.9	*2.1*	1.4	5(23)
kil-2	46	20.1	56	29.3	19.3	47.3	0.77	1.7	63(38)
98080	31.3	18.0	42	18.9	2.9	31.9	*1.28*	0.2	-
127037	20.4	16.4	20	14.8	2.9	19.9	2.8	0.9	-
goethite	1.20	1.20	0	1.12	-2.0	1.35	-	-	-
greig-tw1	33.4	24.8	26	25.4	3.9	47.7	*6.31*	1.9	4(47)
greig-it1	42.6	38.5	10	29.4	0	55.9	6.87	0.9	-(48)
SYNTHETIC SAMPLES of dispersed powders in epoxy resin									
pyr-a	35.0	25.7	27	27.0	6.9	37.4	*2.9*	1.6	83(28)
pyr-b	26.8	19.0	29	18.1	7.8	25.7	*3.2*	1.8	83(30)
magn1a	4.77	2.05	57	2.14	4.2	4.82	0.96	1.8	78(56)
magn6a	94.2	43.3	54	45.2	2.8	103	0.98	1.9	83(56)
magn6c	6.44	2.68	58	-	5.0	6.45	0.84	-	-
magn6d	3.20	1.33	58	1.33	-0.2	3.20	0.88	-	-
iron-2	12.8	2.18	83	1.36	-6.0	11.9	0.22	2.2	20(89)
MD hem	2.33	0.97	58	1.03	3.4	2.52	1.10	1.3	12(59)
SD hem	3.92	2.43	38	2.76	9.3	3.73	1.67	1.06	14(26)

All SIRM and IRM values are expressed in μAm^2; $SIRM_1$ is the initial SIRM of the sample (before compression) in the pressure cell (at zero pressure); IRM_{p2} is residual IRM under maximum pressure p_2=1.24 GPa (inside the cell); Δ (in %) is pressure demagnetization degree under p_2; IRM_{PR} is residual IRM after decompression from p_2 and extraction of the sample from the cell. δ (in %) corresponds to changes in IRM upon decompression from p_2 (IRM decreases when δ is negative and increases when δ is positive). $SIRM_2$ is SIRM acquired after decompression from p_2 and new saturation; MDS is median destructive stress (in GPa); it is italized when linear extrapolation of pressure demagnetization curves was used for MDS determination. In the right column numbers between brackets correspond to ε_0 values at 0 mT (in %). α=[($SIRM_0$-IRM_{p1})/($SIRM_0$-IRM_{p2})]/[p_1/p_2], where p_1=0.46 GPa; ε_1=1-ε(30 mT)/ε_0, where $\varepsilon(B)$=[$IRM_B(B)$-$IRM_{BP}(B)$]/$IRM_B(B)$, ε_0=ε(0 mT) and B is alternating field (see text).

(1) Values of remanent magnetization correspond to the NRM of the cell (that was never saturated);

(2) The initially compressed magnetization was TRM; (3) The initially compressed magnetization was NRM

Table 3. Parameters related to pressure sensitivity of different magnetic mineralogies.

	p_1=0.46 GPa					p_2=1.24 GPa					
Magnetic mineralogy	a_1	b_1	r_1	r_1^*	R^2_1	a_2	b_2	r_2	r_2^*	R^2_2	B_{th} (mT)
pyrrhotite	0.005	0.90	0.38	0.39	0.01	0.06	0.56	0.73	0.71	0.63	110036
nickel iron	0.14	0.42	0.88	0.81	0.82	0.35	-0.49	1.00	0.99	1.00	701
hematite	0.04	0.60	0.53	0.08	0.43	0.11	0.04	0.90	0.59	0.93	6100073
(Ti)magnetite	0.15	0.34	0.65	0.57	0.47	0.27	-0.22	0.74	0.66	0.63	10099

Residual isothermal remanent magnetization under pressure normalized to its initial SIRM (IRM_p) can be calculated for p_1=0.46 GPa and p_2=1.24 GPa using the following empirical equation: $IRM_{px}/SIRM = a_x \cdot \ln(B_{cr}) + b_x$, where x=1 for p_1 and x=2 for p_2; B_{cr} is coercivity of remanence in mT. r_x and r_x^* are Pearson correlation coefficients indicating the strength of linear dependences between $IRM_{px}/SIRM$ and B_{cr} as well as $IRM_{px}/SIRM$ and B_c, respectively. Pearson's correlation is determined as a ration of covariance of the two variables to the product of their standard deviation. B_c is magnetic coercivity. R^2_x is the coefficient of determination (R-squared value), it ranges from 0 to 1 and reveals how closely the logarithmic fit $IRM_{px}=f(B_{cr})$ corresponds to the actual data. The calculated R^2_x ~~and R^2_x are correlation coefficient between IRM_p and B_{cr} and determination coefficient of logarithmic fits $IRM_{px}=f(B_{cr})$. r_x^* is correlation coefficient for the case when B_{cr} is replaced by B_c, where B_c is magnetic coercivity.~~ is not an adjusted R-squared value (the transformed regression model is used for calculations). B_{th} is threshold B_{cr} above which no demagnetization under p_2 is possible. $B_{th} = e^{(1-b)/a}$.

Formatted: English (U.S.)

Formatted: English (U.S.)

Formatted: Font: Italic

Formatted: Subscript

Formatted: Superscript

Formatted: Subscript

Formatted: Font: Italic

Formatted: Subscript

Formatted: Font: Italic

Formatted: Subscript

Formatted: Font: Italic

Formatted: Superscript

TABLES

Table 1

Main magnetic properties of investigated samples.

Sample	Main magnetic carrier and ref.	m	T_C	χ_0	MDF_i	B_{cr}	B_{cr}/B_c	M_s	M_{rs}/M_s
METEORITES									
Martian meteorites									
Los Angeles	Ti-magn [11, 13]	94.3	150	10.3	31	55	1.41	1232	0.49
NWA 1068	pyrrhotite [13, 11]	240.2	*325*	1.3	100	134	1.54	212	0.47
NWA 998	magnetite [13, 11]	20.4	*575*	4.3	25	41	1.73	713	0.24
Ordinary chondrites									
Bensour-6a	taenite [0, 1]	162.0	*450*	154.0	18	33	35.8	3187	0.003
Bensour-i	tetrataenite [0, 1]	23.7	580	-	24	64	1.62	1963	0.16
Bensour-j	tetrataenite [0, 1]	102.4	580	46.8	25	64	1.62	1963	0.16
Pultusk	kamacite [0]	64.2	*760*	600.0	10	27	26.0	303	0.007
Saratov	tetrataenite [0]	54.1	*580*	633.0	70	162	35.8	16540	0.03
Rumuruti chondrites									
NWA 753	pyrrhotite [0, 15]	211.9	*325*	8.7	108	134	1.68	93	0.41
TERRESTRIAL ROCKS AND MINERALS									
Basalts									
ba	Ti-magn [9]	59.5	50	16.1	15	18	3.54	622	0.16
ba (TRM)	Ti-magn [9]	405.0	50	16.1	15	18	3.54	622	0.16
bb-a	Ti-magn [0, 6]	327.8	60/150	16.1	8	14	2.29	866	0.18
bb-a (TRM)	Ti-magn [0, 6]	327.3	60/150	16.1	8	14	2.29	866	0.18
bb-b (NRM)	Ti-magn [0, 6]	392.3	60/150	16.1	9	14	2.29	866	0.18
be-3a	Ti-magn [3, 10]	267.7	245	10.8	13	18	2.57	1700	0.13
pd6-2-1	Ti-magn [0, 8]	30.8	280	109.0	15	27	1.86	1827	0.23
pd6-2-4	Ti-magn [0, 8]	51.2	280	131.0	11	21	1.79	1833	0.21
Andesites									
au1b	Ti-magn [0, 5]	226.2	530	121.4	8	16	4.24	1828	0.03
cug1b	Ti-magn [0, 5]	175.5	550	88.7	7	14	4.65	1048	0.03
osb10b	magnetite [0, 5]	125.3	575	9.74	40	69	2.10	139	0.34
Ignimbrites									
spi3301	Ti-magn [0, 5]	302.8	560	73.0	9	16	2.81	545	0.11
ona12	Ti-magn [0, 5]	109.4	560	45.4	24	44	2.86	787	0.12
spi3903	magnetite [0, 5]	233.0	575	54.1	16	27	2.79	621	0.13
mtd5b	magnetite [0, 5]	162.3	575	93.7	22	40	2.37	1356	0.18
iro8	magnetite [0, 5]	161.0	575	13.6	31	48	2.03	151	0.27
Rhyolites									
rb7a	hematite [16]	238.0	650	0.03	>150	406	3.56	5	0.48
Radiolarites									
radiol-1	hematite [0]	333.5	675	1.4	>150	390	1.21	67	0.68

Sample	Main magnetic carrier and ref.	m	T_C	χ_0	MDF_i	B_{cr}	B_{cr}/B_c	M_s	M_{rs}/M_s
radiol-2	hematite [0]	232.1	675	1.6	>150	347	1.30	74	0.69
Granites									
bf0703	magnetite [0, 2]	304.6	575	11.6	39	68	2.98	165	0.15
bf3201	magnetite [0, 2]	425.5	575	41.3	7	13	7.54	448	0.01
bf9804	magnetite [0, 2]	453.3	575	8.8	13	25	6.01	112	0.03
bf8703	magnetite [0, 2]	228.0	575	3.8	34	61	2.08	76	0.24
Microdiorite									
est	magnetite [4]	320.0	575	13.5	8	19	10.3	128	0.01
Schist									
sb3a	pyrrhotite [4]	243.3	280/320	0.3	17	31	1.29	91	0.50
Jasper									
jas	hematite [0]	210.0	675	4.1	>150	289	1.38	154	0.70
Obsidian									
kil-2	Ti-magn [0]	219.4	142	4.4	21	27	1.34	822	0.45
Minerals (monocrystals)									
98080	pyrrhotite [0, 7]	429	325	11.8	4	4	0.88	1444	0.46
127037	pyrrhotite [0, 7]	24.5	325	6.2	3	7	1.51	5696	0.15
goethite	goethite [0, 14]	320.1	~120	0.3	>150	>9000	-	-	-
Sediments									
greig-tw1	greigite [17]	5.0	*330*	970	59	80	1.38	19470	0.52
greig-it1	greigite [18]	4.1	*330*	1408	52	73	1.45	29073	0.45
SYNTHETIC SAMPLES of dispersed powders in epoxy resin									
pyr-a (20.5; 5.2)	pyrrhotite [0, 12]	33.5	*325*	175	7	17	1.73	-	0.21
pyr-b (13.1; 3.4)	pyrrhotite [0, 12]	32.8	*325*	69.2	11	23	1.51	-	0.32
magn1a (0.3; 0.1)	magnetite [0]	170.0	*575*	15.1	15	32	3.22	-	0.08
magn6a (17.3; 4)	magnetite [0]	73.6	*575*	-	14	28	3.02	-	0.09
magn6c (0.8; 0.2)	magnetite [0]	89.4	*575*	-	15	29	3.03	-	0.09
magn6d (0.5; 0.1)	magnetite [0]	79.4	*575*	-	15	30	3.10	-	0.09
iron-2 (2.5; 0.4)	iron [0]	229.5	753	281	8	22	13.8	-	0.004
MD hem (2.1; 0.5)	hematite [0]	116.1	*675*	0.95	67	33	1.11	-	0.57
SD hem	hematite [0]	155.6	*675*	-	>100	177	1.43	-	0.73

m is mass (in mg). T_C is Curie temperature (in °C); theoretical value when italized. χ_0 is low field magnetic susceptibility (in $10^{-6}m^3/kg$). MDF_i is median destructive field of IRM (in mT): 9T IRM for hematite-bearing and goethite samples and 3T IRM for all other samples. B_c and B_{cr} are magnetic coercivity and coercivity of remanence, respectively (in mT). M_s and M_{rs} are saturation and saturation remanent magnetization (in 10^{-3} Am^2/kg). "Ti-magn" is titanomagnetite. For synthetic samples numbers between brackets (1st column) correspond to estimated mass and volume concentrations of powders in the sample respectively (in %) and mass values correspond to the mass of the whole samples of dispersed powder with epoxy resin matrix. In the second column the information between brackets

corresponds to reference(s) where samples are described and/ or their magnetic properties measured. [(0)] this study; [(1-6)] Gattacceca et al., 2003, 2004, 2006, 2007a, 2007b and 2008, respectively; [(7-8)] Louzada et al., 2007, 2008; [(9-15)] Rochette et al., 1993, 1998, 2001, 2003, 2005a, 2005b, 2008, respectively; [(16)] Vlag. et al., 1997; [(17, 18)] {Horng et al., 1998; Jiang et al., 2001} and {Florindo et al., 1995; Van Dongen et al., 2007}, respectively.

Table 2.

Synthesis of results on pressure demagnetization experiments.

Sample	$SIRM_1$	IRM_{p2}	Δ	IRM_{PR}	δ	$SIRM_2$	**MDS**	α	ε_1
pressure cell [(1)]	0.0343	0.0433	-	-	-	-	-	-	-
METEORITES									
Los Angeles	11.9	9.11	23	3.08	3.1	9.20	*2.5*	1.3	21(67)
NWA 1068	25.3	21.1	17	19.8	3.2	24.6	*3.7*	0.8	36(20)
NWA 998	7.97	7.47	6	6.25	-0.4	7.36	*9.5*	1.1	69(15)
Bensour-6a	1.36	1.10	19	1.01	-3.7	1.57	*3.1*	0.8	80(36)
Bensour-i	6.81	6.60	3	6.49	2.1	6.28	*22.4*	1.3	-
Bensour-j	32.0	30.7	4	30.6	-0.9	32.0	*13.3*	1.0	46(4)
Pultusk	15.3	10.2	33	9.89	0	16.0	*1.8*	1.3	98(38)
Saratov	20.3	19.6	3	18.5	0.5	-	*18.9*	0.8	20(16)
NWA 753	7.80	7.05	10	6.94	1.3	7.65	6.5	1.0	44(9)
TERRESTRIAL ROCKS AND MINERALS									
ba	6.78	3.12	54	3.56	12.5	6.13	1.07	1.7	29(42)
ba [(2)]	5.52	3.64	34	-	10.9	-	*1.7*	1.0	-
bb-a	48.3	24.9	48	25.7	1.9	52.5	*1.26*	1.4	95(51)
bb-a [(2)]	2.12	1.11	48	1.63	5.1	52.5	*1.26*	1.5	4(97)
bb-b [(3)]	1.62	0.96	40	0.91	9.1	2.12	1.5	1.0	72(57)
be-3a	74.9	32.1	57	36.9	6.8	71.7	1.08	-	91(48)
pd6-2-1	12.1	8.51	30	8.91	3.9	12.1	*2.6*	1.5	99(26)
pd6-2-4	18.5	11.1	40	10.6	2.2	19.1	*1.6*	1.4	97(45)
au1b	13.1	7.55	42	7.62	0.3	12.7	*1.4*	1.3	-
cug1b	5.62	3.04	46	2.62	-6.9	5.92	*1.29*	1.2	88(56)
osb10b	5.64	3.89	31	4.22	5.7	5.91	2.6	1.6	59(29)
spi 3301	19.1	13.2	31	10.4	-7.3	16.5	*1.9*	1.3	81(37)
ona12	10.4	8.91	14	8.72	0.2	10.4	*4.2*	1.1	89(16)
spi3903	18.1	12.4	31	12.1	1.7	18.3	*2.7*	1.6	75(34)
mtd5b	38.0	33.0	13	37.5	-3.9	37.2	*5.1*	1.4	75(19)
iro8	6.37	6.05	5	5.73	-0.2	6.20	12.4	0.8	88(8)
rb7a	0.55	0.40	27	0.44	8.9	0.60	*2.1*	1.2	14(27)
radiol-1	17.9	11.9	34	11.7	0.0	18.7	*2.3*	1.7	3(38)
radiol-2	13.2	8.53	35	9.45	8.1	13.5	*2.0*	1.7	6(30)
bf0703	9.47	8.22	13	7.80	-2.5	8.47	*4.7*	1.1	-
bf3201	2.76	0.95	66	0.75	-4.6	2.72	0.54	1.8	65(73)
bf9804	1.41	0.77	46	0.73	-3.9	1.54	*1.5*	1.7	66(53)
bf8703	4.14	3.92	5	3.79	-1.7	4.13	*11.9*	1.2	61(8)
est	8.09	1.32	84	0.98	-0.5	8.17	0.19	2.4	43(88)
sb3a	15.5	12.2	22	11.8	5.8	20.3	3.7	0.9	25(42)

Sample	$SIRM_1$	IRM_{p2}	Δ	IRM_{PR}	δ	$SIRM_2$	MDS	α	ε_1
jas	24.3	16.9	30	18.2	6.6	23.9	*2.1*	1.4	5(23)
kil-2	46	20.1	56	29.3	19.3	47.3	0.77	1.7	63(38)
98080	31.3	18.0	42	18.9	2.9	31.9	*1.28*	0.2	-
127037	20.4	16.4	20	14.8	2.9	19.9	2.8	0.9	-
goethite	1.20	1.20	0	1.12	-2.0	1.35	-	-	-
greig-tw1	33.4	24.8	26	25.4	3.9	47.7	*6.31*	1.9	4(47)
greig-it1	42.6	38.5	10	29.4	0	55.9	6.87	0.9	-(48)
SYNTHETIC SAMPLES of dispersed powders in epoxy resin									
pyr-a	35.0	25.7	27	27.0	6.9	37.4	*2.9*	1.6	83(28)
pyr-b	26.8	19.0	29	18.1	7.8	25.7	*3.2*	1.8	83(30)
magn1a	4.77	2.05	57	2.14	4.2	4.82	0.96	1.8	78(56)
magn6a	94.2	43.3	54	45.2	2.8	103	0.98	1.9	83(56)
magn6c	6.44	2.68	58	-	5.0	6.45	0.84	-	-
magn6d	3.20	1.33	58	1.33	-0.2	3.20	0.88	-	-
iron-2	12.8	2.18	83	1.36	-6.0	11.9	0.22	2.2	20(89)
MD hem	2.33	0.97	58	1.03	3.4	2.52	1.10	1.3	12(59)
SD hem	3.92	2.43	38	2.76	9.3	3.73	1.67	1.06	14(26)

All SIRM and IRM values are expressed in μAm^2; $SIRM_1$ is the initial SIRM of the sample (before compression) in the pressure cell (at zero pressure); IRM_{p2} is residual IRM under maximum pressure p_2=1.24 GPa (inside the cell); Δ (in %) is pressure demagnetization degree under p_2; IRM_{PR} is residual IRM after decompression from p_2 and extraction of the sample from the cell. δ (in %) corresponds to changes in IRM upon decompression from p_2 (IRM decreases when δ is negative and increases when δ is positive). $SIRM_2$ is SIRM acquired after decompression from p_2 and new saturation; MDS is median destructive stress (in GPa); it is italized when linear extrapolation of pressure demagnetization curves was used for MDS determination. In the right column numbers between brackets correspond to ε_0 values at 0 mT (in %). α=[($SIRM_0$-IRM_{p1})/($SIRM_0$-IRM_{p2})]/[p_1/p_2], where p_1=0.46 GPa; ε_1=1-ε(30 mT)/ε_0, where $\varepsilon(B)$=[$IRM_B(B)$-$IRM_{BP}(B)$]/$IRM_B(B)$, ε_0=ε(0 mT) and B is alternating field (see text).

(1) Values of remanent magnetization correspond to the NRM of the cell (that was never saturated);

(2) The initially compressed magnetization was TRM; (3) The initially compressed magnetization was NRM

Table 3. Parameters related to pressure sensitivity of different magnetic mineralogies.

	p_1=0.46 GPa					p_2=1.24 GPa					
Magnetic mineralogy	a_1	b_1	r_1	r_1^*	R^2_1	a_2	b_2	r_2	r_2^*	R^2_2	B_{th} (mT)
pyrrhotite	0.005	0.90	0.38	0.39	0.01	0.06	0.56	0.73	0.71	0.63	1100
nickel iron	0.14	0.42	0.88	0.81	0.82	0.35	-0.49	1.00	0.99	1.00	70
hematite	0.04	0.60	0.53	0.08	0.43	0.11	0.04	0.90	0.59	0.93	6100
(Ti)magnetite	0.15	0.34	0.65	0.57	0.47	0.27	-0.22	0.74	0.66	0.63	100

Residual isothermal remanent magnetization under pressure normalized to its initial SIRM (IRM_p) can be calculated for p_1=0.46 GPa and p_2=1.24 GPa using the following empirical equation: $IRM_{px}/\text{SIRM} = a_x \cdot \ln(B_{cr}) + b_x$, where x=1 for p_1 and x=2 for p_2; B_{cr} is coercivity of remanence in mT. r_x and r_x^* are Pearson correlation coefficients indicating the strength of linear dependences between IRM_{px}/SIRM and B_{cr} as well as IRM_{px}/SIRM and B_c, respectively. Pearson's correlation is determined as a ration of covariance of the two variables to the product of their standard deviation. B_c is magnetic coercivity. R^2_x is the coefficient of determination (R-squared value), it ranges from 0 to 1 and reveals how closely the logarithmic fit $IRM_{px}=f(B_{cr})$ corresponds to the actual data. The calculated R^2 is not an adjusted R-squared value (the transformed regression model is used for calculations). B_{th} is threshold B_{cr} above which no demagnetization under p_2 is possible. $B_{th} = e^{(1-b)/a}$.